Barometer-Assisted 3D Indoor WiFi Localization for Smart Devices

- Map Selection and Performance Evaluation

by

Julang Ying

A Thesis

Submitted to the Faculty

of the

WORCESTER POLYTECHNIC INSTITUTE

In partial fulfillment of the requirements for the

Degree of Master of Science

in

Electrical and Computer Engineering

by

May 2016

APPROVED:

Professor Kaveh Pahlavan, Major Thesis Advisor, ECE Department

---

Professor Emmanuel Agu, Committee Member, CS Department

Professor Andrew Clark, Committee Member, ECE Department

Professor Allen H. Levesque, Committee Member, ECE Department

---

Professor Yehia Massoud, Head of Department

Abstract

Recently, indoor localization becomes a hot topic no matter in industry or academic field. Smart phones are good candidates for localization since they are carrying various sensors such as GPS, Wi-Fi, accelerometer, barometer and etc, which can be used to estimate the current location. But there are still many challenges for 3D indoor geolocation using smart phones, among which the map selection and 3D performance evaluation problems are the most common and crucial.

In the indoor environment, the popular outdoor Google maps cannot be utilized since we need maps showing the layout of every individual floor. Also, layout of different floors differ from one another. Therefore, algorithms are required to detect whether we are inside or outside a building and determine on which floor we are located so that an appropriate map can be selected accordingly.

For Wi-Fi based indoor localization, the performance of location estimation is closely related to the algorithms and deployment that we are using. It is difficult to find out a general approach that can be used to evaluate any localization system. On one hand, since the RF signal will suffer extra loss when traveling through the ceilings between floors, its propagation property will be different from the empirical ones and consequently we should design a new propagation model for 3D scenarios. On the other hand, properties of sensors are unique so that corresponding models are required before we analyze the localization scheme. In-depth investigation on the possible hybrid are also needed in case more than one sensor is operated in the localization system.

In this thesis, we firstly designed two algorithms to use GPS signal for detecting whether the smart device is operating inside or outside a building, which is

called outdoor-indoor transition detection. We also design another algorithm to use barometer data for determining on which floor are we located, which is considered as a multi-floor transition detection. With three scenarios designed inside the Akwater Kent Laboratory building (AK building) at Worcester Polytechnic Institute (WPI), we collected raw data from an Android phone with a version of 4.3 and conducted experimental analysis based on that. An efficient way to quantitatively evaluate the 3D localization systems is using Cramer-Rao Lower Bound (CRLB), which is considered as the lower bound of the estimated error for any localization system. The characteristics of Wi-Fi and barometer signals are explored and proper models are introduced as a foundation. Then we extended the 2D CRLB into a 3D format so that it can fit the our 3D scenarios. A barometer-assisted CRLB is introduced as an improvement for the existing Wi-Fi Receive Signal Strength (RSS)-only scheme and both of the two schemes are compared with the contours in every scenario and the statistical analysis.

Acknowledgements

In this thesis, I describe the research I conducted in pursuit of my Master of Science Degree in Electrical & Computer Engineering in Worcester Polytechnic Institute.

Firstly, I would like to offer my most sincerely gratitude to my research advisor, Prof. Kaveh Pahlavan, for leading me into the research world, for sharing his wisdom no matter in doing research and daily life. He can always offer his help whenever he can afford and give me guide to go through the difficulties I met in the study.

I'm really grateful that I can have Prof. Emmanuel Agu, Prof. Andrew Clark and Prof. Allen H. Levesque as my committee members. Thank you for the valuable comments and reviewing of this thesis.

I also want thank all the peers in lab CWINS, Yishuang Geng, Bader, Zhouchi Li, Chao Ren and Yang Yang. Thank these people so much that they offer me such a nice atmosphere in the lab like a family.

At last, I would like to delicate my thesis to my beloved parents and my wife, who offer me totally understanding, support and infinite love.

Contents

List of Figures

List of Tables

Chapter 1

Background

Smart devices have become essential parts of our daily life. Smart phone owners can not only use their phones to make phone calls, but also access a wide range of services and information. They can read breaking news, conduct transaction through online banking, and even get information about their health condition from the small but smart devices. Another important application of smart phones is localization and navigation. With various embedded sensors, location can be estimated by different techniques which makes smart phone a good candidate for both outdoor and indoor geolocation. GPS is reliable and accurate in the outdoor localization. By acquiring the Line-of-Sight from the satellites, location can be calculated by using triangulation. Other sensors can also be utilized for indoor localization, such as Wi-Fi, barometer, accelerometer, gyroscope and etc. Wi-Fi signal is the most popular technique that is used in the indoor localization. From the received signal strength (RSS) or time of arrival (ToA), distance from the access points (APs) can be calculated and triangulation can be applied to acquire the estimated location as well. Barometer is good in determine the height of the user inside the building, since altitude is closely related to the air pressure measured by the barometer. Accelerometer

is used for measuring the acceleration of the movement. By calculating the second integral of the acceleration, distance of movement can be calculated. Gyroscope is helpful in detecting motion and by looking into the data gathered from this sensor, every motion can be detected so that the location can be estimated according to that.

Although indoor geolocation has been explored for a couple of years, there are still challenging problems in this area, among which the map selection and performance evaluation problem are the most crucial and critical. The commonly used Google maps have good performance in the outdoor localization and navigation. By using Google maps, one can be guided to a place with high speed and accuracy GPS application. However, the Google maps do not pay much attention to the indoor environment, in which the detailed layout should be displayed. So it is crucial for us to find out whether the smart phone is operating in the outdoor or indoor environment and the correct map can be selected accordingly. Also, in multiple-floor buildings, layout differs from different floors. Therefore, we should also find out the which floor the smart phone user is currently located in so that the corresponding map can be displayed. The first part of the map selection problem can be described as outdoor-indoor transition detection and the second part as multi-floor transition detection. To solve these to detection problems, proper sensor selection is the very first step, after which scenarios and algorithms can be designed and consequently experiments can be conducted.

For any indoor geolocation problem, it equally important to evaluate the performance. It is essential since a criterion is needed for designing algorithm and deploying the APs so that we can compare different techniques that are used and choose the one with the best performance. But there are still some challenging issues related to this problem. A general and efficient way should be provided and

we can utilize it to analyze any indoor geolocation system. The approach can also be modified since for different localization schemes, other sensors will be fused and the modified scheme is able to respond to any change.

This thesis investigates and presents approaches to solve the two problems described above. Firstly we design two algorithms using Global Positioning System (GPS) signal to detect whether the smart phone is operating inside or outside of a building and compare these two algorithms with the performance of false alarm and time delay. Then we introduce another algorithm using data from barometer to detect transition between floors inside a building. Thirdly, we provide models for the behavior of Wi-Fi Received Signal Strength (RSS) and barometric data. With those models, the accuracy of 3D Wi-Fi localization and barometer-assisted Wi-Fi localization can be evaluated by calculating Cramer-Rao Lower Bound (CRLB).

1.1 Related Works

Since smart phone is powerful with various embedded sensors (Barometer, Gyroscope, etc.) and other applications (WiFi, GPS), approach for intruder detection can be implemented in multiple methods. Some related work has been done related to this topic.

The work described by [7] presents an approach which detects intruder for WLAN access. Least Mean Square (LMS) and Prioritized Maximum Power (PMP) are used as two RSS-based matching algorithms. Their performance of accuracy are compared in indoor and outdoor-indoor areas and PMP algorithm provides a better performance than LMS in positioning application.

An approach using fusion of sensors, WLAN signals and building information for

indoor/campus localization is developed by [8]. This method shows the possibilities of combing the measurements from different sensors and building information to obtain accurate indoor localization as well as the possibilities that sensors can aid in intruder detection[9].

Some indoor personal navigation applications are introduced in [6]. Map Matching Algorithms are implemented, which make the Pedestrian Navigation Module (PNM) have the capbility to provide localization results even with bad reception of GPS signals.

Another approach is described in [7] which fuse dead reckoning (DR) algorithm, GPS, and RFID for pedestrian positioning. This method is implemented as software module with web-based APIs on computing systems which shows that GPS and the active RFID tag system can seamlessly and effectively adjust estimation errors in DR as well as possibilities for sensor fusion localization.

1.2 Contribution

This thesis includes two major chapters and the main two contributions are listed as follows:

- Introduce the map selection problem, and explore methods to solve it. Two algorithms are designed to use LoS satellite number from GPS data for detecting the outdoor-indoor transition and another algorithm is applied to use barometric data for detecting the multiple-floor transition. Detection efficiency is evaluated from the aspects of false alarm and time delay.

- Introduce the performance evaluation problem, and find out an approach to quantitatively analyze 3D Wi-Fi localization systems. Properties of Wi-Fi

RSS is investigated and a 3D path loss model is designed to describe signal propagation. Barometer is used to improve the localization performance and modeled with a Gaussian distribution. By extending the 2D CRLB into 3D, RSS-only localization scheme and Barometer-assisted scheme are compared.

1.3 Thesis Outline

In the following chapter, we will review some general concepts of 3D indoor geolocation. Chapter 3 describes the methodology we use to solve the map selection problem based on the GPS and barometer signals. The approaches for 3D indoor localization performance evaluation are outlined in Chapter 4 while conclusion and future work are presented in Chapter 5.

Chapter 2

Test Bed, State Machine Design and Sensor Selection

2.1 Introduction

In 3D indoor environment, the localization problem becomes extremely complicated. The first consideration is the difference between the techniques utilized in indoor and outdoor geolocation systems. The widely used GPS is no longer an option for the indoor environment since it requires LOS which is blocked in most situations. Many new techniques have been explored recently. The most used one is RF-based technique. Since the properties of RF signals like Received Signal Strength (RSS) and Time-of-Arrival (ToA) can be utilized to determine to the distance between the transmitter and receiver. Then the triangulation can be applied to find out the location of the mobile points (MPs). Recently, more sensor are introduced into the area of indoor geolocation, such as accelerometer, gyroscope, and barometer, which is commonly described as sensor-fusion techniques. Moreover, since most of the building will have cameras all over the building for security purposes, the image

processing techniques can also be applied in the indoor geolocation area. Another consideration is the difference in the maps used in the outdoor and indoor environment. The Google map can be acquired easily when the users are in the outdoor environment with high-accurate outdoor geolocation. But when one comes indoor, the outdoor map is no longer accurate enough since the outdoor maps cannot show the detailed structure of the indoor environment on different floors and the transition between floors. So indoor maps should be used instead. The last consideration is the 3D geolocation vs 2D geolocation schemes. There have been large amount of researches conducted for the 2D geolocation. But when it comes to 3D scenarios, the problem becomes more complex. For example, the WiFi signal will suffer extra loss when going through the ceilings between floors and the pass loss model should be changed accordingly. In the 2D scenarios, every estimated location is on a certain floor. But in 3D scenarios, more information should be applied such as how to whether the user is inside or outside the building, on which floor is the user located and whether the user is in the elevator or on the stair.

From the considerations above, it is crucial to look deeply into the 3D indoor geolocation problems from different aspects.

2.2 Test Bed and State Machine Design

2.2.1 Test-bed

Test-bed is inside and outside the Atwater Kent (AK) building in Worcester Polytechnic Institute (WPI). The experiments are mainly composed two parts: the first is mainly focusing on the spots around three doors (shown and labeled in Figure on the first floor; the second part is mainly measuring barometric pressure on different floors under different mode and detecting floor changing using pressure-height

formula.

We conducted several experiments using Android phone (version 4.3) to collect GPS data and barometric pressure data. Matlab is used to do data analysis and conduct various performance evaluation simulations.

2.2.2 State Machine Design

Since the map is selected according to the current state (indoor/outdoor or different floors), a state machine model satisfies the problem perfectly. A state machine is designed with four states according to the building structure of AK building: outdoor and indoor (1st floor, 2nd floor and 3rd floor). Note that when the state goes from the outdoor to the indoor state, the state machine will go to the 1st floor state since one will be on the 1st floor when enter the building. There are two types of transitions between the indoor states: elevator and stair, since the user may either walk the stairs or take the elevator to go between floors.

With all the four states and triggering conditions for transition, the entire state machine is depicted in Figure 2.1.

2.3 Sensor Selection

Now that the four states are determined, suitable sensors should be selected from which data can be provided to predict the transition between different states. Commonly, modern smart phones are integrated with various sensors, such as embedded GPS radio, accelerometer, gyroscope, barometer, and etc. We tested all the sensors in outdoor, indoor and multi-floor scenarios and found GPS radio the best to determine indoor/outdoor transition while barometer the best to determine

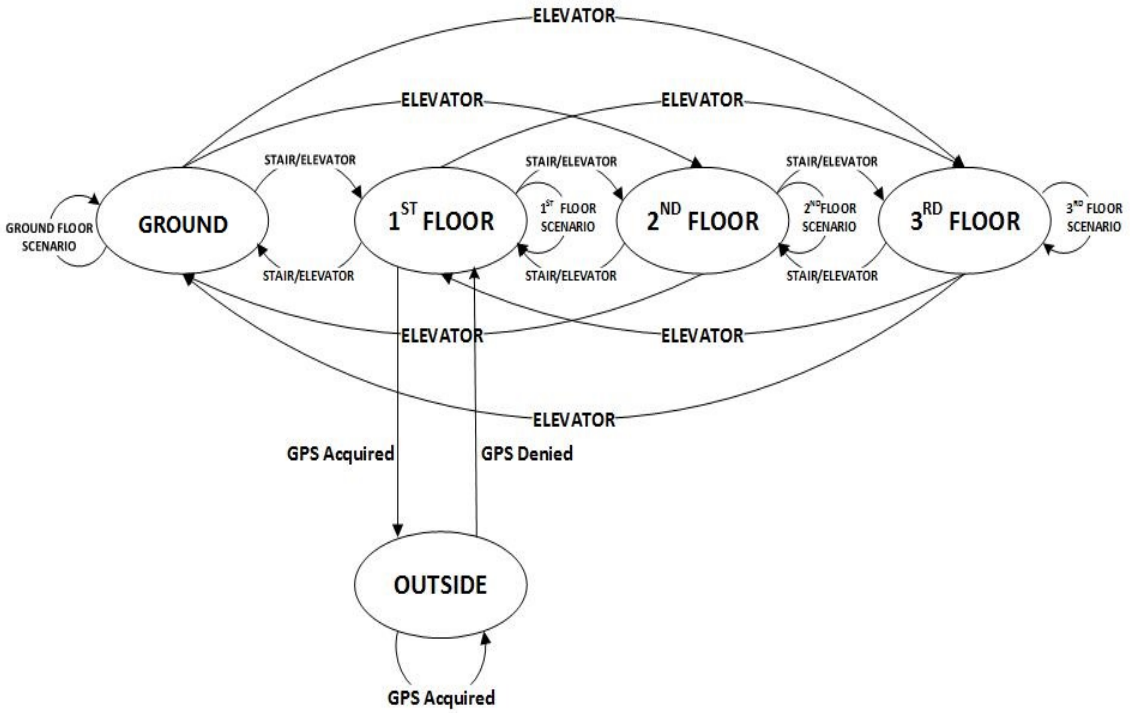

Figure 2.1: State Machine

multi-floor transition.

Detection of indoor/outdoor transition will be made according to the availability of GPS radio. It's well recognized that GPS provides great accuracy in outdoor localization. But the signal is lost in most indoor environments which are hostile to GPS radio. So we can roughly determine the user is outdoor when GPS is acquired and indoor when GPS is denied. But the detection is not accurate enough in all cases, so some methods are discussed to improve the performance in the next section.

As for detection of floor transition, we exploit the properties of barometric pressure since it is tightly related to the altitude of each floor (can be calculated by using certain equations). When the user is going upstairs or downstairs, he can choose either walking the staircase or taking the elevator. These two methods show

different characters in the barometric pressure readings, so we should treat them differently. More exploration will be presented in the pressure-height model.

Chapter 3

Map Selection Problem in 3D Indoor Environment

3.1 Introduction

In the highly-developing society, smart phones with accurate and reliable Global Positioning System (GPS) can easily leads you to the right place. However, outdoor navigation alone cannot meets people's needs to reach certain places, especially when the destinations are located at some complicated indoor environments such as schools or hospitals, where the ubiquitous GPS is challenged[1][2][3][4][5]. To implement indoor navigation[6], not only new equipment and technologies should be used, but outdoor maps should be replaced with indoor maps. Moreover, maps of different floors in multi-floor buildings differ from each other, which makes it more complex to choose a proper map. Then here comes the map selection problem: if one is going from outdoors to indoors, or going between different floors inside a building, how can the maps be selected automatically to serve the accurate and in-time navigation.

This map selection problem can be divided into two parts: outdoor-indoor transition and multi-floor transition. For the first part, decision should be made to determine whether the user is indoor or outdoor (can be viewed as intruder detection problem)and the corresponding map should be selected as soon as the current condition changes. For the second part, detection should be made to determine which floor is the user located at a specific time and the map should be selected to represent the correct floor.

There exists some difficulties in making the decision precise and in-time:

- Different buildings have different geometry (doors, corridors, and windows) and equipment (stair and elevator), which makes it extremely complex to detect transition.

- Smart phones have various sensors, and we should decide what sensors can be used to solve the problem and whether they can be fused for better performance.

In this chapter, we present a standard method which can be used to solve automated map selection problem, for either outdoor-indoor or multi-floor transition detection. We also design several algorithms according to the data gathered from the sensors, compare their performance, and give an general solution. We aim to develop a simple and state-of-the-art approach which can be used into smart phone application in the future.

3.2 Experimental Setup

The experiment is conducted on different floors inside AK building. The detailed scenarios design and data collection methods will be discussed below.

3.2.1 Scenarios Design and Data Collection for Outdoor-Indoor Transition

Three scenarios are designed for the outdoor-indoor transition detection, each of which is around 3 doors on the 1st floor in AK building. The location of the three doors are shown in Figure 3.1.

- Scenario 1: Door 1 (Out, Out-In, In)
- Scenario 2: Door 2 (Out, Out-In, In)
- Scenario 3: Door 3 (Out, Out-In, In)

In each scenario, three types of movement data are included and collected, which are walking around the door outside the building (Out), walking through the door (Out-In) and walking around the door inside the building (In).

For this part of experiments, GPS signal data is collected from the Android phone in every 10ms. The database is consisted with the number of LoS satellite and location estimation in every sampling spot. Given this database, we are able to evaluate the estimation error in every location and the performance of the GPS in indoor geolocation. What's more, we can also design classification algorithms to analyze the number of LoS satellite and detect outdoor-indoor transition.

3.2.2 Scenarios Design and Data Collection for Multi-Floor Transition

Another three scenarios are designed for the multi-floor transition detection, which are conducted on three floors, in the elevator or on the stairs.

Figure 3.1: Scenarios at Three Doors

- Scenario 1: Same floor (1st, 2nd and 3rd floor)
- Scenario 2: Floor transition by stair
- Scenario 3: Floor transition by elevator

In Scenario 1, we collect barometric data

3.3 Outdoor-Indoor Transition Detection

As is mentioned above, GPS radio is considered the best for detecting outdoor-indoor transition. From the embedded GPS radio, we can get both the Line-Of-Sight (LOS) satellite number and the estimated location at a certain moment. From these two types of data, we can design algorithms to realize transition detection.

The first arithmetical design is based on the availability of the GPS radio. State is recognized as outdoor if GPS is acquired while indoor if GPS is denied. To get a precise location estimation, more than 4 LOS satellites should be available. So

at the beginning of the algorithm, we should make sure that more than 4 LOS satellites is acquired. If not, the algorithm will not work until the LOS satellite number meets the requirement. To detect the transition, we should also consider the building geometry. Since entrances of a building are the access between outdoor and indoor world, we should pay special attention to the data gathered around the door. Consequently, the location should be around the entrance before we make a transition detection and we will ignore all the changes of the GPS status when we are far from the entrance.

The basic structure of the algorithm is shown as Figure 3.2. It starts by receiving the GPS signal from the phone, and compares the received LOS satellites number with 4. If the LOS satellite number is more than 4(including 4), we have enough number of signals to estimate our current location and calculate the distance from the door. If so, the value of distance will be updated and we will compare the calculated distance with a predefined threshold. If the distance is within the threshold, then we can go to the next step and the system attempts to make a decision to change the state.

The state change problem is similar to the handover problem in cellular network [10], so we design two handover algorithms for this part.

The easiest and most direct way to make a handover decision is using the availability of the GPS signal. The steps of Algorithm 1 are depicted in Figure 3.3. The state will change if the GPS status changes. If GPS signal is available, we decide the state as outdoor; If GPS signal is denied, we decide it as indoor.

Algorithm 1 is simple and straight, but it has great disadvantage since it will introduce numbers of false alarms, especially when the device is around the door and the GPS signal keeps changing frequently. We add some improvement in Algorithm 2 (shown in Figure 3.4) and the state will not change until GPS status stays the

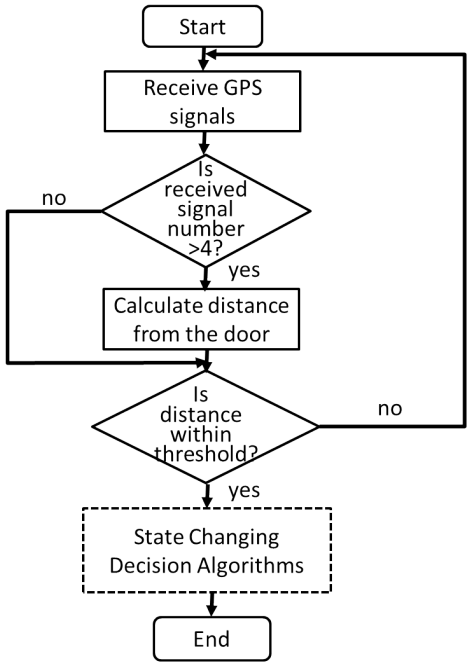

Figure 3.2: Basic structure of the algorithm

same for a certain period of time. The decision not only depends on the current status of GPS signal, but the maintenance of the GPS signal.

3.4 Multi-Floor Transition Detection

Detection of floor transition should be considered in another way since the barometric pressure readings has a different property from the satellite data. A pressure-height model is constructed so that we can calculate the altitude of a certain location from which the floor transition can be determined. What's more, new algorithms are explored to eliminate the effect of some factors (noise, bias) in the pressure-height model and analyze the transition progress. The following two sections will discuss more about these two aspects.

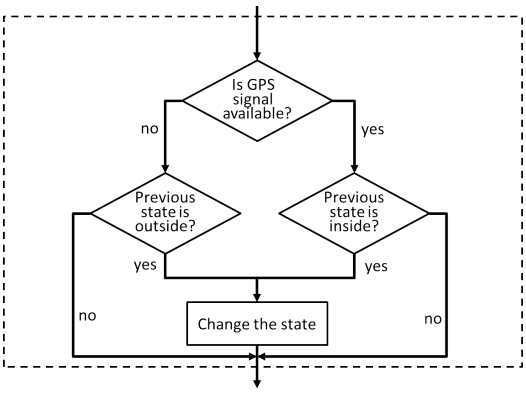

Figure 3.3: Decision algorithm 1: using only GPS access to make the decision

Pressure-height Model

Barometric pressure is exploited for detecting multi-floor transition since it is related to the altitude of the current location. According to the International Standard Atmosphere Model formulated by International Civil Aviation Organization, their relation can be represented and derived by equation 4.12.

$$\begin{aligned} p &= p_0 \times (1 - \frac{L \times h}{T_0})^{\frac{g \times M}{R \times L}} \\ &\approx p_0 \times (1 - \frac{g \times h}{c_p \times T_0})^{\frac{c_p \times M}{R}} \\ &\approx p_0 \times exp(\frac{-g \times M \times h}{R \times T_0}) \end{aligned} \tag{3.1}$$

All the parameters used in the pressure-height equation is shown in Table 4.1. From the equation above, altitude can be calculated from barometric pressure, which is derived as follow:

$$h = -\frac{R \times T_0}{g \times M} \times ln(\frac{p}{p_0}) \tag{3.2}$$

Basically, we can calculate altitude from air pressure according to equation 3.2, however, data gathered from the smart phone suffers great noise, bias, and time difference, which will affect the precision of the transition detection. The following

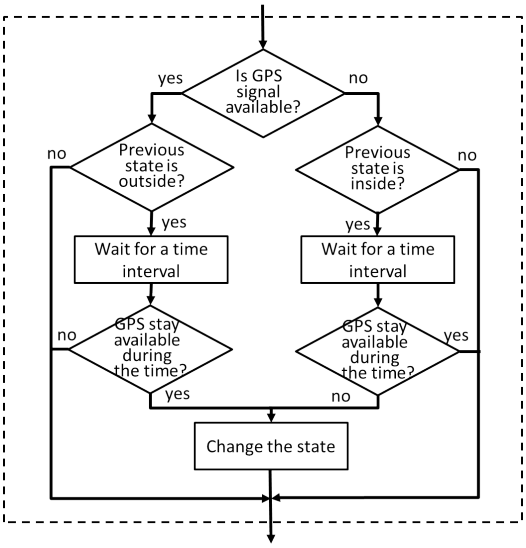

Figure 3.4: Decision algorithm 2: using GPS access and time delay to make the decision

Table 3.1: Parameters used in pressure-height equation

Parameter	Description	Value
p_0	Standard atmospheric pressure	101325 Pa
L	Temperature lapse rate	0.0065 K/m
c_p	Constant pressure specific heat	1007 J/kg*K
T_0	Sea level standard temperature	288.15 K
g	Gravitational acceleration	9.80665 m/s^2
M	Molar mass of dry air	0.0289644 kg/mol
R	Universal gas constant	8.31447 J/(mol*K)

three sections will have a deeper look at these three factors.

Noise causes the change of raw pressure readings in a fixed floor. This change is slow with a small range, and after fitting it into different distributions (shown in Figure 3.5), we find it an ideal Gaussian-distributed noise with zero mean (white noise). To eliminate the effect of noise, we use a simple low-pass filter, which will be discussed later.

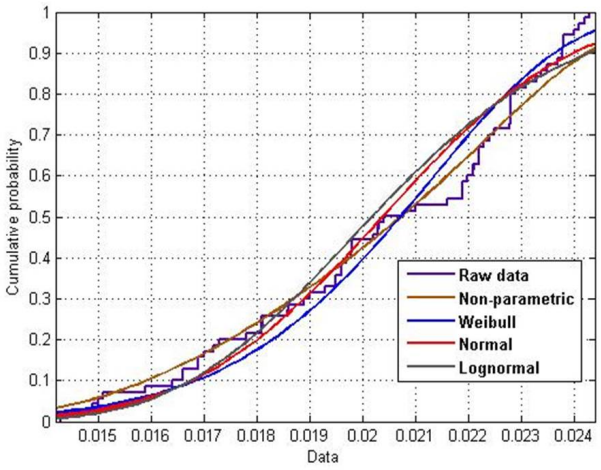

Figure 3.6: Distribution fit for bias

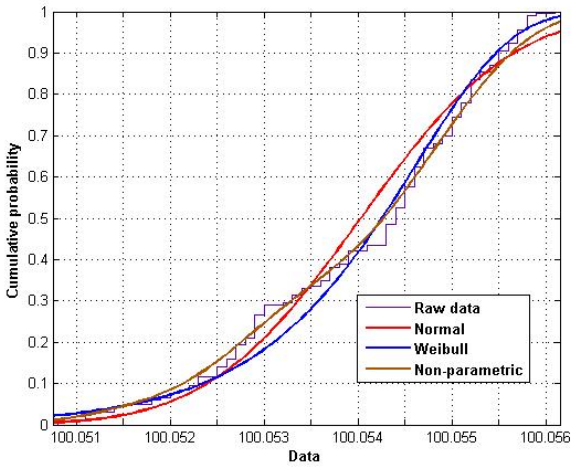

Figure 3.5: Distribution fit for noise

Bias is the difference of raw pressure reading caused by different devices. In our experiment, we use two different barometers to measure the air pressure and fit their difference with different distributions (shown in Figure 3.6). We find that bias is also Gaussian-distributed with a certain mean value. Note that although we can model bias between different devices, in reality we don't need to put it into consideration in localization. The reason is that during the navigation, the device

is fixed and we don't need to know the difference.

Time difference is the most uncertain part in the pressure-height model. From equation 4.12we can see that some physical factors will affect the barometric pressure, such as temperature and humidity (which will change during the time), then at different time, we will get pressure data with extremely great difference. For example, the barometric pressure in winter is much higher than that in summer in a fixed place at the same time during a day.

Fortunately, when we are using the model to deal with localization, we can assume that the time duration is so small that we don't need to consider time difference anymore.

When noise, bias and time difference are considered, the equation should be written as follow:

$$h' = -\frac{D \times R \times T_0}{g \times M} \times ln(\frac{p + N + B}{p_0}) \tag{3.3}$$

Where N represents noise, B represents bias and D represents time difference.

Smoothing

Since raw pressure reading contains some noises, which may distort the result and affect threshold value choice, and thus influence the detection of floor transfer. To eliminate those noise, we adopt double exponential smoothing to produce smoothed data. The basic idea of double exponential smoothing is to take account of the trend estimation, this technique works as follows: x_t is the raw data set, $s_t$is the smoothed value set, $b_t$is the best estimation value of the trend. For initial value,

$$\begin{aligned} s_1 &= x_1 \\ b_1 &= x_1 - x_0 \end{aligned} \tag{3.4}$$

And for $t > 1$,

$$\begin{aligned} s_t &= \alpha \times x_t + (1 - \alpha) \times (s_{t-1} + b_{t-1}) \\ b_t &= \beta \times (s_t - s_{t-1}) + (1 - \beta) \times b_{t-1} \end{aligned} \tag{3.5}$$

α is the data smoothing factor, $0 < \alpha < 1$, and is the trend smoothing factor, $0 < \beta < 1$. The smoothing factor means how much recent changes weights to result. In this case, factor values close to zero have more smoothing effect and are more responsive to recent changes. Considering the distortion and calibration, we use 0.3 for α and 0.2 for β. It effectively removes the noisy peak and showed smoothed readings.

Algorithms for Detection

The algorithm used for transition detection is quite similar with the ones used for intruder problem, the difference lies in that we use the pressure readings variance as the parameter that used as the threshold to determine floor transition.

To identify whether it is a floor transition mode or not, we just need to figure out prominently pressure variance, which can be realized by applying 1st derivation to pressure reading and setting thresholds. After smoothing the derivative result, there is still some noise and transient oscillation, which might cause bias and effect detection accuracy. The main basis of floor detection is comparing derivative result with threshold, therefore identifying the transition. According to that, we should compare period result behavior with threshold value and avoid transient oscillation influence. And setting a D_buffer, which to store 1st derivative value in a 15 seconds period, could effectively solve our problem. The D_buffer is triggered every 5 seconds. And after analysis the result data, we find both in stair mode and elevation mode, the threshold could be 1.3. If there are 10 data value in the

Algorithms for floor transition detection

```
        Num_sample <-- number of qualified samples in 15-sec-
ond buffer
        DEM <-- Double exponential smoothing
        DEV <-- 1st derivation
Inputs:  P <-- raw pressure value
    D-raw <-- 1st pressure derivation value
    D_buffer <-- 15 second buffer of 1st pressure derivation
value
Outputs:  FLOOR_CHANGED state
THRESH1 <-- 1.3(threshold of 1st pressure derivation value)
THRESH_EXCEED <-- false
C_Dev <-- DEV(P)
D_filt <--DEM(C_Dev)

IF (D_filt > THRESH1)
    THRESH_EXCEED == TRUE
END IF
(Every five seconds triggers D_buffer starts from current
second, during the buffer period)
FOR i=1:1:15
     IF(THRESH_EXCEED)
     Num_sample = Num_sample + 1
     END IF
  IF Num_sample >=10
  THEN return FLOOR_CHANGED
  END IF
```

Figure 3.7: Floor detection algorithm

buffer are larger than threshold, then transient value influence minimized and floor transition identified. The algorithm is shown in Figure 3.7 in detail.

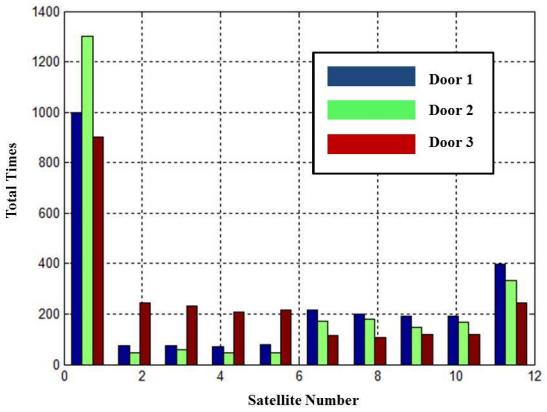

Figure 3.8: Histogram of the GPS signal in the database

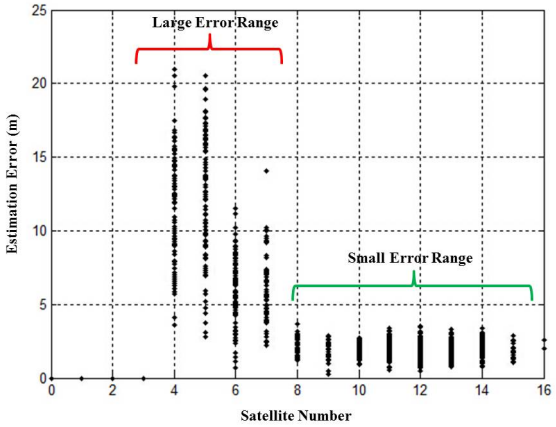

Figure 3.9: Error range of the estimation by using different number of satellites

3.5 Results and Analysis

3.5.1 Histogram, Error Range & CDF of Estimation Error

The histogram for different LOS GPS satellite number is shown in Figure 3.8. We can see that three doors show different GPS signal characters in the histogram. The difference comes from the different geometry of these doors. There are various factor which affects the geometry: the number of doors, the opening shape and the surroundings (especially windows).

From estimated location in a certain location, we can find the estimation error in this position and relate the error to the LOS satellite number in the position we can have the error range shown in Figure 3.9. From the plot we can see that when we only get 4 or 5 LOS satellites in one position, the estimated location becomes inaccuracy while we have more than 6 LOS satellites, the error range falls and accuracy increases.

Plot cumulative distribution function (CDF) of the estimation error vs LOS satellites number in Figure 3.10. We make satellite number into two groups, one with more than 4 LOS satellites while the other only has 3 or 4 LOS satellites. We can see in the plot that with greater LOS satellite number, we have better estimation error performance.

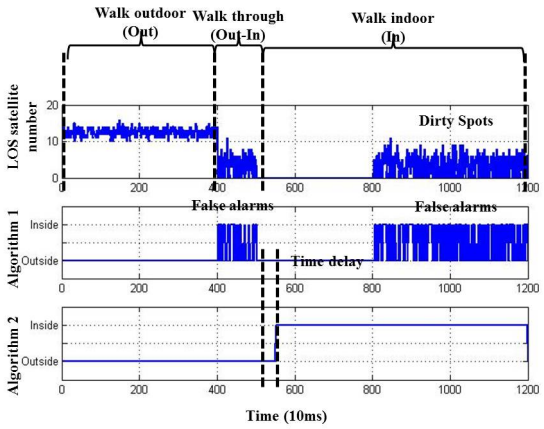

Figure 3.13: State decision when going around Door 3

3.5.2 Performance Comparison of Algorithms

Figure 3.11-3.13 show the intruder detecting progress. The first plot in every figure shows the original data (LOS satellite number) at every position while walking in the scenario. The second and third plots are the detection results of Algorithm 1 and 2 respectively. We can see clearly that for Algorithm 1, there are always great number of false alarms since the GPS status changes frequently while we are walking through a door. Algorithm 2 shows significant improvement in eliminating the false alarms. However, it introduces some delay, which degrades the continuity of the system.

Dirty spots in the scenario of Door 3 greatly affect the detection accuracy. We can see in Fig. 11 that even if we are indoor, the LOS satellite number remains to a certain scale that which brings lots of false alarms. To eliminate the effect, we should make a large wait time to make sure that the current state is stable. As long as the state is decided as stable, we can make a accurate detection.

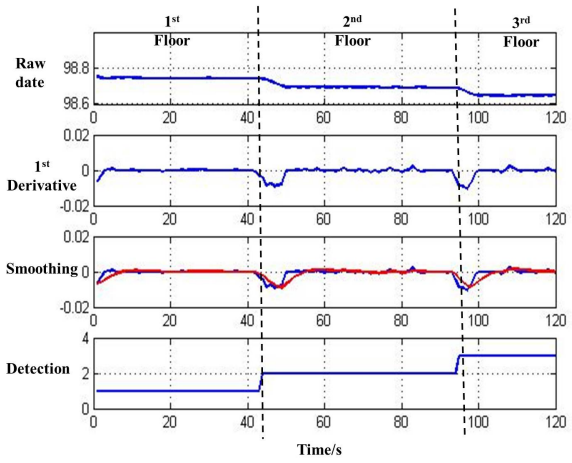

Figure 3.14: Floor decision for elevator

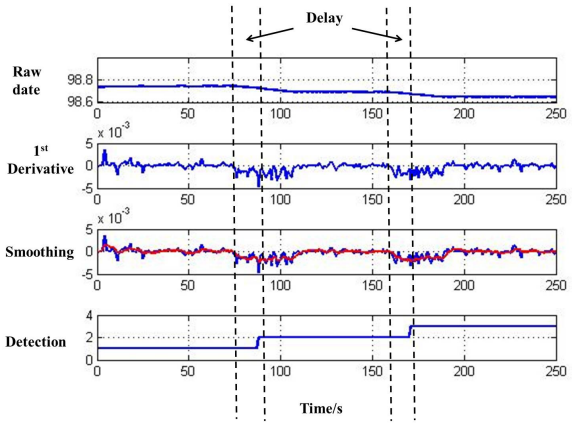

Figure 3.15: Floor decision for stair

Figure 3.14 and 3.15 show the multi-floor detection progress for elevator and stairs. The first plot in every figure shows the original data (air pressure) at every position while walking in the scenario. The second and third plots are first derivative and its smoothing respectively. We can see clearly that after smoothing, it is more clear for us to see the transition between two floors. The fourth plot shows the detection results by using the algorithms described above.

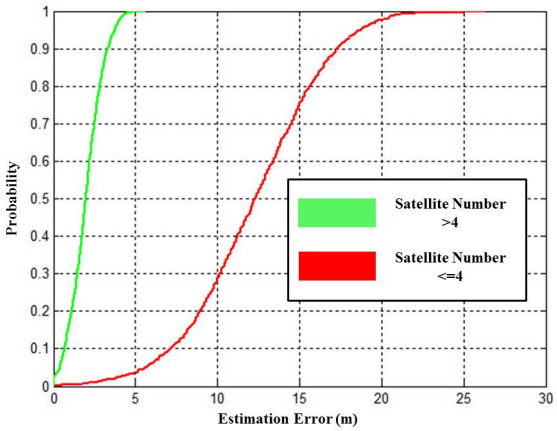

Figure 3.10: CDF plot of the estimation error by using different number of satellites

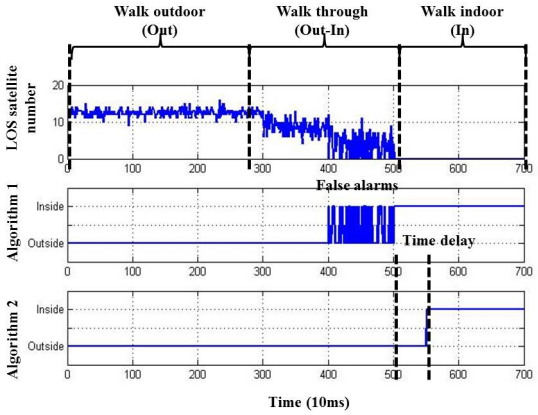

Figure 3.11: State decision when going around Door 1

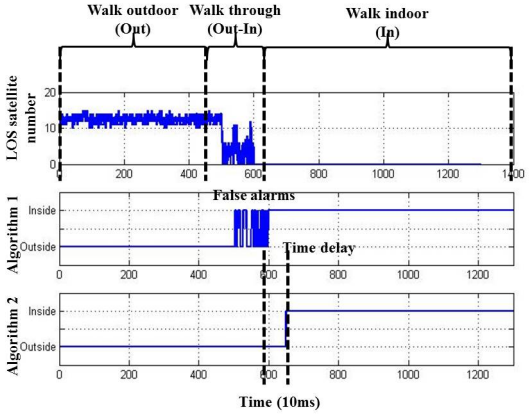

Figure 3.12: State decision when going around Door 2

Chapter 4

Performance Evaluation Methods for 3D Indoor Geolocation

4.1 Introduction

The patient safety and clinical risk issue have attracted increasing focus and one of the best ways to manage them is to let the hospital staff know the precise location of the in-patients. People have developed many approaches and systems to track and identify the in-patients so that the health care can be offered immediately.

Received Signal Strength (RSS) is most widely used in the indoor geolocation since it can be measured by various applications and consequently data set is easily set up. But the RSS-based method cannot provide as accurate estimation as TOA-based technique does since the indoor radio channel suffers from severe multi-path propagation and shadow fading [15–17]. RFId provides another approach that can be used for tracking and identifying patients [4, 5]. Sensor-fusion is also frequently explored to assist the existing geolocation systems and brings in improvement to the performance [6, 7]. Recently, researches have been conducted by using the hot

iBeacon technique for in-room newborns localization in hospital which opens a new world for accurate localization in Line-of-Sight (LOS) small areas [8].

In this chapter, we are trying to explore how barometer can assist the existing 2D RSS-based geolocation system so that the inaccurate vertical estimation is eliminated and a better 3D localization system is created. Then we design scenarios and calculate 3D CRLB in these situations to evaluate their performance. The general idea of the 3D CRLB is similar to some previous researches [8, 9], but the focus of our study is on the entire building which has the widest range while others are focusing on the in-body or in-room localization, which have a smaller range.
The patient safety and clinical risk issue have attracted increasing focus and one of the best ways to manage them is to let the hospital staff know the precise location of the in-patients. People have developed many approaches and systems to track and identify the in-patients so that the health care can be offered immediately.

4.2 Experimental Setup

4.2.1 Scenarios Design

To compare different geolocation systems, the very first step is to design test scenarios so that their performance can be evaluated in a same way.

We have designed 3 scenarios in which APs are deployed in multiple floors:

- 5 APs are placed on the ceiling of the same floor (4 at each corner and 1 in the middle).
- Another 5 APs are placed on the 2nd floor in the same way and we have signals from 10 APs in total.

- Extra 5 APs are placed on the 3rd floor in the same way and we have signals from 15 APs in total.

We assume that every floor has a space of 30m×30m and a height of 5 meter. Every floor is sampled in every 0.1 meter (the 4 edges are not includes), so we have $299 \times 299 = 89401$ samples in total.

4.3 RSS-Only CRLB Calculation

As mentioned before, 2D indoor geolocation has been well researched and various signals have been used to obtain the current location, among which RSS is the most widely used one. To characterize the signal, a suitable path-loss model should be chosen. The empirical 2D path-loss [10] is shown as follow

$$P_r(r) = P_0 - 10\alpha \log_{10} r \tag{4.1}$$

Where α is the gradient indicating the relation between distance and power and r is the distance from the transmitter to the receiver. In the environment of a hospital, the materials of the buildings are brick, wood, metal, and other composites. These materials have different gradients from 2 to 6. It's crucial to use a suitable α according to different environment.

The RSS will suffer extra loss while going through the ceilings in 3D environment, we should add penalty to the empirical 2D path-loss model. We define $P_f(n)$ as the path loss when signal is going through the ceilings. Shadow fading should also be considered, which is defined as $D(f)$ and can be modeled as a white noise, where f represents the transmitting frequency. Then the modified path-loss model

can be written as:

$$P_r(r) = P_0 - 10\alpha(r)\log_{10} r - P_f(n) + D(f) \tag{4.2}$$

In the simulation with the IEEE 802.11b,g standard, we operate the transmitting frequency as 2.4GHz, the power of transmitter as 20dBm (100mW) and P_0 is approximately -20dBm. We also adopt the well-known distance-partitioned path loss model to determine the power gradient α, which is simply related to the distance. If r is less than 10 meters, we make $\alpha = 2$; If r is more than 10 meters but less than 20 meters, α becomes 3; If r is larger than 20 meters, then α is 6. For the function of $P_f(n)$, the JTC model is applied, which is given as $15 + 4(n-1)$, where n indicates the number of ceilings. Both models are well described in [10]

Then the 3D path-loss model for every floor of three scenarios is given as:

$$P_r(r) = -20 - \begin{cases} 20log_{10}r - P_f(n) & (10 \geq r \geq 0) \\ 30log_{10}r - P_f(n) & (20 \geq r > 10) \\ 60log_{10}r - P_f(n) & (r > 20) \end{cases} \tag{4.3}$$

As long as we have the path loss model, we can explore the characteristic of the received signal strength. Since we can easily get power observations from different Access Points (APs), a received power matrix $\boldsymbol{P}$ can be generated, with an assumption of N deployed APs and m observations from each AP [12]. In this 3D path loss model, the distance between the transmitter and receiver should be calculated in a 3D way, which is $r_i = \sqrt{(x-x_i)^2 + (y-y_i)^2 + (z-z_i)^2}$, where (x, y, z) and (x_i, y_i, z_i) represent the location of the AP and ith receiver respectively,

$i = 1, 2, 3, ..., m$. We can use the equation below for illustration:

$$\mathbf{P} = \mathbf{G}\boldsymbol{\beta} \tag{4.4}$$

Where

$$\boldsymbol{P} = \begin{bmatrix} P(r_1) \\ P(r_2) \\ \vdots \\ P(r_m) \end{bmatrix}, \boldsymbol{G} = \begin{bmatrix} 1 & \alpha(r_1)log(r_1) & P_f(n) \\ 1 & \alpha(r_2)log(r_2) & P_f(n) \\ \vdots & \vdots & \vdots \\ 1 & \alpha(r_m)log(r_m) & P_f(n) \end{bmatrix}, \boldsymbol{\beta} = \begin{bmatrix} P_0 \\ -10 \\ -1 \end{bmatrix}$$

The matrix of $\boldsymbol{G}$ and $\boldsymbol{\beta}$ should be modified from the original equation [12] since the JTC model have been applied to the modified path loss model.

The least-square estimate of the unknown parameter vector $\hat{\boldsymbol{\beta}}$ is given by

$$\hat{\boldsymbol{\beta}} = (\boldsymbol{G}'\boldsymbol{G})^{-1}\boldsymbol{G}'\boldsymbol{P} \tag{4.5}$$

The standard deviation of the received power σ_p is written as follow

$$\sigma_p = \sqrt{\frac{1}{m}(\boldsymbol{P}' - \hat{\boldsymbol{\beta}}'\boldsymbol{G}')\boldsymbol{P}} \tag{4.6}$$

To analyze the relation between RSS and the least location error (CRLB), we can apply partial differential to Equation (4.1) [8, 9]. Then we have

$$dP_i(x, y, z) = -\frac{10\alpha}{ln10}(\frac{x - x_i}{r_i^2}dx + \frac{y - y_i}{r_i^2}dy + \frac{z - z_i}{r_i^2}dz) \tag{4.7}$$

We can also write this equation in a matrix format, which is

$$d\boldsymbol{P} = \boldsymbol{H} \cdot d\boldsymbol{r} \tag{4.8}$$

where

$$d\boldsymbol{r} = \begin{bmatrix} dx \\ dy \\ dz \end{bmatrix}, \boldsymbol{H} = \begin{bmatrix} -\frac{10\alpha}{ln10}\frac{x-x_1}{r_1^2} & -\frac{10\alpha}{ln10}\frac{y-y_1}{r_1^2} & -\frac{10\alpha}{ln10}\frac{z-z_1}{r_1^2} \\ -\frac{10\alpha}{ln10}\frac{x-x_2}{r_2^2} & -\frac{10\alpha}{ln10}\frac{y-y_2}{r_2^2} & -\frac{10\alpha}{ln10}\frac{z-z_2}{r_2^2} \\ \vdots & \vdots & \vdots \\ -\frac{10\alpha}{ln10}\frac{x-x_N}{r_N^2} & -\frac{10\alpha}{ln10}\frac{y-y_N}{r_N^2} & -\frac{10\alpha}{ln10}\frac{z-z_N}{r_N^2} \end{bmatrix}$$

By using the same least-square estimation method we mentioned before, estimation of the location error can be evaluated:

$$d\boldsymbol{r} = (\boldsymbol{H}'\boldsymbol{H})^{-1}\boldsymbol{H}'d\boldsymbol{P} \tag{4.9}$$

and the covariance matrix of the location error is

$$cov(d\boldsymbol{r}) = \sigma_P^2(\boldsymbol{H}'\boldsymbol{H})^{-1} = \begin{bmatrix} \sigma_x^2 & \sigma_{xy}^2 & \sigma_{xz}^2 \\ \sigma_{xy}^2 & \sigma_y^2 & \sigma_{yz}^2 \\ \sigma_{xz}^2 & \sigma_{yz}^2 & \sigma_z^2 \end{bmatrix} \tag{4.10}$$

Then the CRLB can be calculated as follow:

$$\sigma_r = \sqrt{\sigma_x^2 + \sigma_y^2 + \sigma_z^2} \tag{4.11}$$

4.4 Barometer-Assisted CRLB Calculation

For 3D localization, more information is needed since the RSS signal suffered great loss when going through the ceilings between floors. With the assistance of barometer, we can collect air pressure of the current location which relates closely to the altitude. The relation is called Pressure-Height physical law and can be

Table 4.1: Parameters used in pressure-height equation

Parameter	Description	Value
p_0	Standard atmospheric pressure	101325 Pa
L	Temperature lapse rate	0.0065 K/m
c_p	Constant pressure specific heat	1007 J/kg*K
T_0	Sea level standard temperature	288.15 K
g	Gravitational acceleration	9.80665 m/s^2
M	Molar mass of dry air	0.0289644 kg/mol
R	Universal gas constant	8.31447 J/(mol*K)

expressed as follow [13]:

$$\begin{aligned} p &= p_0 \cdot (1 - \frac{L \cdot h}{T_0})^{\frac{g \cdot M}{R \cdot L}} \\ &\approx p_0 \cdot (1 - \frac{g \cdot h}{c_p \cdot T_0})^{\frac{c_p \cdot M}{R}} \\ &\approx p_0 \cdot e^{\frac{-g \cdot M \cdot h}{R \cdot T_0}} \end{aligned} \tag{4.12}$$

Where p represents the air pressure and h the altitude. All the parameters used in the pressure-height equation is shown in Table 4.1.

We use the embedded barometer in smart phone and record its measurements while going round the floor, which is shown in Figure 1(A). Then we find that the CDF of barometric data is perfectly fit to a normal distribution (see in Figure 1(B)) with a standard deviation of $\sigma_b = 4.1424Pa$ with which we can estimate the altitude.

In this case, assume that we have a parameter of height h and the function of $p(h)$. We can also obtain observations of air pressure $\boldsymbol{O}$. In the observation, a Gaussian noise will be included with a zero mean as well as a variance of ${\sigma_b}^2$.

$$\boldsymbol{O} = p(h) + \boldsymbol{N} \tag{4.13}$$

So the probability distribution function of the observation can be written as

$$f(\boldsymbol{O}|h) = \frac{1}{\sqrt{2\pi}\sigma_b} e^{\frac{(\boldsymbol{O}-p(h))^2}{2{\sigma_b}^2}} \tag{4.14}$$

To calculate the CRLB of parameter in a function, the Fishers information matrix should be calculated, which can be written as follow:

$$\begin{aligned}
\boldsymbol{F} &= E[\frac{\partial}{\partial h}\{lnf(\boldsymbol{O}|h)\}]^2 \\
&= E[\frac{\partial}{\partial h}\{-ln\sqrt{2\pi}\sigma_b - \frac{(\boldsymbol{O}-p(h)^2)}{2\sigma_b^2}\}]^2 \\
&= E[\frac{(\boldsymbol{O}-p(h))\cdot p'(h)}{\sigma_b^2}]^2 \\
&= \frac{{p'(h)}^2}{\sigma_b^4} \cdot E[\boldsymbol{O}^2 - 2\boldsymbol{O}p(h) + {p(h)}^2] \\
&= \frac{{p'(h)}^2}{\sigma_b^4} \cdot \{E[\boldsymbol{O}^2] - 2E[\boldsymbol{O}]\cdot p(h) + p(h)^2\}
\end{aligned} \tag{4.15}$$

Since $E[\boldsymbol{O}] = p(h)$ and $E[\boldsymbol{O}^2] = E[\boldsymbol{O}]^2 + \sigma_b^2 = p(h)^2 + \sigma_b^2$, then the equation comes to:

$$\boldsymbol{F} = \frac{{p'(h)}^2}{\sigma_b^2} \tag{4.16}$$

Moreover, we have:

$$\begin{aligned}
p'(h) &= \frac{\partial}{\partial h}\{p_0 \cdot e^{\frac{-g\cdot M\cdot h}{R\cdot T_0}}\} \\
&= -\frac{g\cdot M\cdot p_0}{R\cdot T_0} e^{\frac{-g\cdot M\cdot h}{R\cdot T_0}}
\end{aligned} \tag{4.17}$$

And $-\frac{g\cdot M}{R\cdot T_0}$ can be denoted as K.Then the Cramer-Rao Lower Bound of the barometer can be calculated as follow:

$$\sigma_h^2 = \boldsymbol{F}^{-1} = \frac{\sigma_b^2}{p'(h)^2} = \frac{\sigma_b^2}{Kp_0\cdot e^{Kh}} \tag{4.18}$$

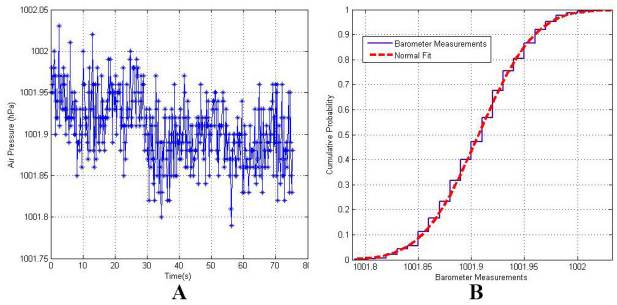

Figure 4.1: Barometer Measurements (A) & Normal Fit of CDF (B)

Since $\sigma_b = 4.1424Pa$ and we also have the value of all the parameters, we can calculate σ_h in different height. But in reality, σ_h does not change much when the altitude is less than 1000 meters. With a σ_b of 4.1424, σ_h is approximately 0.3469 meter, which is much smaller than the vertical one in the RSS-only covariance matrix (in an order of several meters). Consequently, it is reasonable if we replace the original σ_z with σ_h, which will definitely increase the accuracy. Then the barometer-assisted CRLB is derived as:

$$\sigma_r = \sqrt{\sigma_x^2 + \sigma_y^2 + \sigma_h^2} \tag{4.19}$$

4.5 Results and Analysis

In this section, we will present the results and give our analysis from which conclusions can be made.

4.5.1 Contours of CRLB in Three Scenarios

We illustrate the contours of CRLB for the three Scenarios in Figure 2-4. In the figures, characteristic of error performance is clearly presented.

Note that although the space is 30m $\times$ 30m, we do not include the observations on the edges. Consequently, the contour shows a $29.9m \times 29.9m$ space instead of a $30m \times 30m$ one.

4.5.2 CDFs of Different Scenarios

When we explore more about the statistical characteristic of the performance, we illustrate the CDFs of different scenarios under both RSS-only and Barometer-assisted CRLB, which is shown in Figure 5.

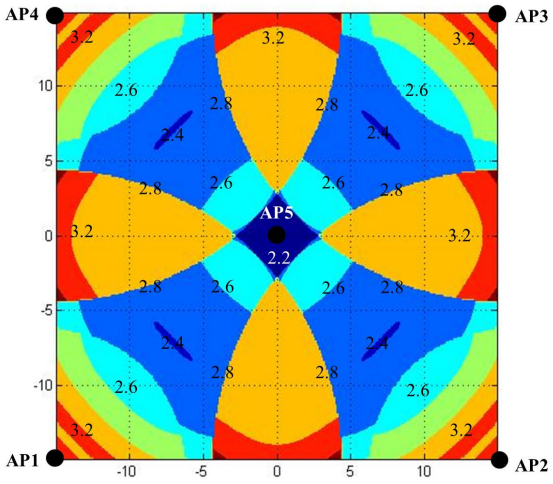

Figure 4.2: Contour of CRLB in Scenario 1

From the figure, we can see that the location error is decreased when more information from other floors is applied. Moreover, if the barometer assist the calculation of the CRLB, the performance is greatly improved.

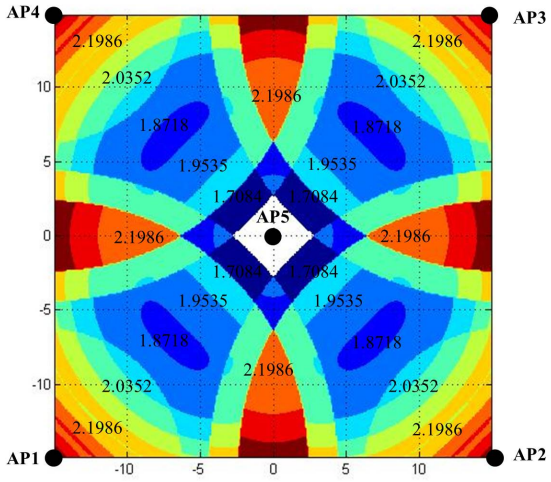

Figure 4.3: Contour of CRLB in Scenario 2

4.5.3 Barometer-Assisted Method vs. RSS-Only Method

Maximum, minimum, and mean CRLB value of the three scenarios using these two methods are listed in Table II. From the table, we can find that by adopting the barometer-assisted method, a 41.67%, 29.29%, and 19.20% improvement can be achieved under the Scenarios 1, 2, and 3 respectively.

Table 4.2: Barometer-Assisted Method vs. RSS-Only Method in Error Performance

CRLB (m)	Maximum	Minimum	Mean
Scenario 1 (Baro)	3.4641	2.1274	2.8113
Scenario 1 (RSS)	7.2791	2.5492	4.8193
Scenario 2 (Baro)	2.5254	1.6267	2.0658
Scenario 2 (RSS)	4.2394	1.9236	2.9214
Scenario 3 (Baro)	2.1120	1.3761	1.7286
Scenario 3 (RSS)	2.9488	1.5440	2.1393

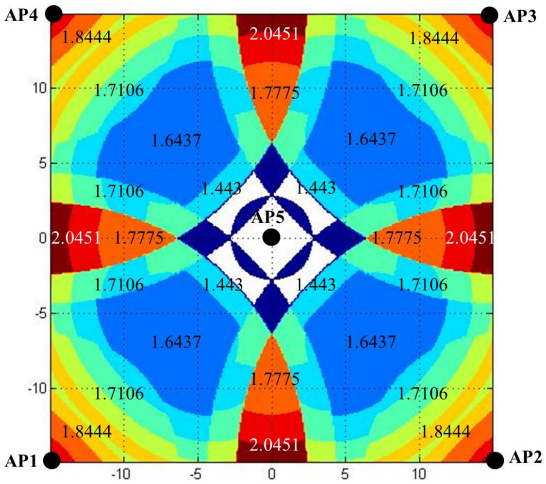

Figure 4.4: Contour of CRLB in Scenario 3

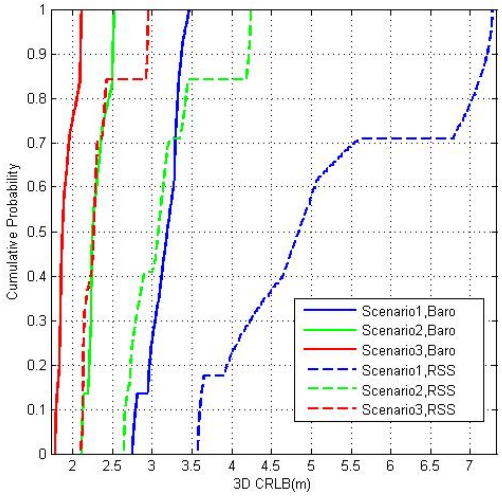

Figure 4.5: CDFs for Three Scenarios

Chapter 5

Performance Evaluation Methods Concerning Coverage Probability and Variable Shadow Fading

5.1 Introduction

As described in the previous chapter, CRLB gives a bound of the estimated location error, which can be used for evaluating the performance of geolocation systems. But in the procedure of signal transmission, other factors should also be considered, one of which is the coverage certainty. When the signal is transmitted, it is possible that its power may go below the sensitivity of the receiver. When the noise it suffers has the opposite angle and degrades the power of the signal, the power reaches the receiver may go below the device sensibility. In this case, we should consider the effect In the evaluation of geolocation systems, other factors also play an important role to determine the performance of various systems, no matter what technologies or algorithms they've used. In this chapter, probability of

coverage will be considered into the previously-discussed RSS-based CRLB. We all know that the signal reaching the receiver is not a hundred percent readable since it suffers from shadow fading during the transmission. According to the path loss model defined in the previous chapter, we can derive the probability of coverage of certain transmission and with which a weighted CRLB can be calculated to evaluate the performance of scenarios concerning the matter of coverage probability.

5.2 Experimental Setups

To compare different geolocation systems, the very first step is to design test scenarios so that their performance can be evaluated in a same way.

We have designed 5 scenarios which can be divided into two types, 2D scenarios and 3D scenarios. The first 3 scenarios are designed on the same floor and we can compare these 3 scenarios for the effects of AP number. In Scenario 4 and 5, APs are deployed in multiple floors, and we can compare the effect of 3D scenarios. The detailed scenario description is given as follow:

- Scenario 1: 3 APs are placed on the ceiling of the same floor (at 3 of the 4 corners).
- Scenario 2: 4 APs are placed on the ceiling of the same floor (at the 4 corners).
- Scenario 3: 5 APs are placed on the ceiling of the same floor (at the 4 corners and the middle).
- Scenario 4: 4 APs are placed on the ceiling of the 3rd floor (at the 4 corners), and we calculate the total CRLBs of the three floors.
- Scenario 5: 4 APs are placed on the ceiling of every floor (at the 4 corners, 12 APs in total), and we calculate the total CRLBs of the three floors.

We assume that every floor has a space of 30m×30m and a height of 5 meter. Every floor is sampled in every 0.1 meter (the 4 edges are not includes), so we have $299 \times 299 = 89401$ samples in total for every scenario.

5.3 Probability of Coverage

To analyze the coverage certainty, we should start from the commonly used path loss model in decibels, which is given by:

$$L_p = L_0 + 10\alpha \log_{10} r \tag{5.1}$$

Where L_p is the total path loss from the transmitter to receiver. L_0 is the normalized path loss, which is the power loss at 1 m. α is the gradient indicating the relation between distance and power. In the environment of office buildings, the materials of the buildings are brick, wood, metal, and other composites. These materials have different gradients from 2 to 6. In large office area, α is changeable according to different r, which indicates the distance from the transmitter to the receiver.

The transmitted signal is also expected to have different path losses in different directions, causing power variation when it reaches to receiver. This variation is commonly called shadow fading or large-scale fading since its cause is obstruction by objects around the receiver. It is not feasible to model shadow fading in a deterministic way, and therefore we usually use statistical models instead. We define l as the shadow fading in the radio propagation, which is a zero mean normally distributed random variable with a standard deviation of σ. The probability

distribution function (PDF) for shadow fading can be written as:

$$f(l) = \frac{1}{\sqrt{2\pi}\sigma} e^{-l^2/2\sigma^2} \tag{5.2}$$

Every receiver has its own sensitivity, which is the minimum RSS that it can recognize. Given the PDF of the shadow fading, we can calculate the probability that the RSS in one location will be lower that the sensitivity (Outage) as well as the probability that it is higher than the sensitivity (Coverage). It is obvious that the sum of the two will be one and we only need calculate one of them. We denote s as the difference between transmitted power and the sensitivity, which indicates the maximum power loss for effective transmission. Then the probability of coverage can be derived as follow:

$$\begin{aligned} Prob(Coverage) &= Prob(L_p + l < s) = Prob(l < s - L_p) \\ &= 1 - \int_{s-L_p}^{\infty} f(l)dl \\ &= 1 - \int_{s-L_p}^{\infty} \frac{1}{\sqrt{2\pi}\sigma} e^{-l^2/2\sigma^2} dl \\ &= 1 - \frac{1}{2} erfc(\frac{s - L_p}{\sqrt{2}\sigma}) \end{aligned} \tag{5.3}$$

Where $erfc()$ is the complementary error function, and $erfc(x) = \frac{2}{\sqrt{\pi}} \int_x^{\infty} e^{-t^2} dt$. Then we can replace L_p with Equation (1), and the coverage probability is written as:

$$Prob(Coverage) = 1 - \frac{1}{2} erfc(\frac{s - L_0 - 10\alpha \log_{10} r}{\sqrt{2}\sigma}) \tag{5.4}$$

From Equation (5.4), we can see that all the factors are constant except d,

which means that the probability is a function of the distance between the transmitter and receiver.

5.4 Weighted CRLB Calculation

5.4.1 Cramer-Rao Lower Bound

Cramer-Rao Lower Bound (CRLB) indicates the smallest estimation error under given observations and is frequently used in evaluating the performance of localization systems. In order to investigate the relation between the location error and signal strength error, we apply a differential operation to both sides of Equation (5.1) with respect to two coordinates x and y, then we have:

$$dL_{pi}(x,y) = \frac{10\alpha_i}{ln10}(\frac{x-x_i}{r_i^2}dx + \frac{y-y_i}{r_i^2}dy), i = 1,2,...,N \tag{5.5}$$

where L_{pi} is the total path loss from AP_i to the location of (x,y); (x_i,y_i) is the coordinate of AP_i; α_i is the power-distance gradient for signal coming from AP_i; r_i is the distance between the receiver and AP_i, and $r_i = \sqrt{(x-x_i)^2+(y-y_i)^2}$; N is the number of APs.

The set of Equation (5.5) can be written in matrix form as:

$$d\boldsymbol{L_p} = \boldsymbol{H} \cdot d\boldsymbol{r} \tag{5.6}$$

Where

$$d\boldsymbol{L_p} = \begin{bmatrix} dL_{p1} \\ dL_{p2} \\ \vdots \\ dL_{pi} \end{bmatrix}, d\boldsymbol{r} = \begin{bmatrix} dx \\ dy \end{bmatrix}, \boldsymbol{H} = \begin{bmatrix} \frac{10\alpha}{ln10}\frac{x-x_1}{r_1^2} & \frac{10\alpha}{ln10}\frac{y-y_1}{r_1^2} \\ \frac{10\alpha}{ln10}\frac{x-x_2}{r_2^2} & \frac{10\alpha}{ln10}\frac{y-y_2}{r_2^2} \\ \vdots & \vdots \\ \frac{10\alpha}{ln10}\frac{x-x_N}{r_N^2} & \frac{10\alpha}{ln10}\frac{y-y_N}{r_N^2} \end{bmatrix}$$

From Equation (5.6), we can estimate the location error.

$$d\boldsymbol{r} = (\boldsymbol{H'H})^{-1}\boldsymbol{H'}d\boldsymbol{L_p} \tag{5.7}$$

Since the path loss estimation error is identical to the error caused by shadow fading, which has zero mean and variance of σ^2, and these errors for different APs are independent with each other, then we can have the two equations as follow:

$$\boldsymbol{E}[d\boldsymbol{L_{pi}}] = 0, cov(d\boldsymbol{L_{pi}}, d\boldsymbol{L_{pj}}) = \begin{cases} \sigma^2, i = j \\ \qquad\qquad i, j = 1, 2, ..., N \\ 0, i \neq j \end{cases} \tag{5.8}$$

Then the covariance matrix of the location error $d\boldsymbol{r}$ is given by

$$cov(d\boldsymbol{r}) = \sigma^2(\boldsymbol{H'H}) = \begin{bmatrix} \sigma_x^2 & \sigma_{xy}^2 \\ \sigma_{xy}^2 & \sigma_y^2 \end{bmatrix} \tag{5.9}$$

The standard deviation of location error is finally derived as

$$\sigma_r = \sqrt{\sigma_x^2 + \sigma_y^2} \tag{5.10}$$

From Equation (5.10), we can see that if the transmission environment is given, the location error only relies on the coordination of the receiver (x, y), and we can calculate the CRLB at any location according to that.

The usage of matrix only fits the condition that there are more than 2 APs. If only one AP is available, another method should be applied instead.

In this case, the partial differential equation should be:

$$dL_{pi}(r) = \frac{10\alpha_i}{ln10}\frac{dr}{r}, i = 1, 2, ..., N \tag{5.11}$$

Then the location error can be estimated as follow:

$$dr = \frac{ln10 \cdot r}{10\alpha_i} dL_p i(r), i = 1, 2, ..., N \tag{5.12}$$

And covariance of dr can be derived:

$$\begin{aligned} cov(dr) &= (\frac{ln10 \cdot r}{10\alpha_i})^2 cov(dL_p i(r)) \\ &= \sigma^2 (\frac{ln10 \cdot r}{10\alpha_i})^2, i = 1, 2, ..., N \end{aligned} \tag{5.13}$$

which is also the variance of dr, so the CRLB in this case is

$$\sigma_r = \frac{ln10 \cdot r}{10\alpha_i}\sigma, i = 1, 2, ..., N \tag{5.14}$$

5.4.2 2D CRLB Concerning Coverage Certainty

From the previous section, we can calculate the probability that a location can be covered by a AP as well as the CRLB which shows the minimum location error under this condition. It is reasonable for us that calculate the CRLB concerning the effect of coverage certainty, so that the total CRLB will be more reliable and accurate.

We denote p_i as the probability that a certain location can be covered by AP_i, which can be calculated by Equation (5.4). Suppose there are N APs in total, the

probability that k APs are covered can be calculated according to the probabilities we calculated before. The number of combinations C of selecting k elements out of N can be calculated as

$$C = \begin{pmatrix} N \\ k \end{pmatrix} = \frac{N!}{k!(N-k)!} = \frac{N(N-1)\cdots(N-k+1)}{k(k-1)\cdots 1}$$

To calculated the CRLB concerning coverage certainty, all the probabilities for the combinations should be explored and the total CRLB should be the summation of every individual CRLB times its corresponding probability. For example, if only 1 AP is covered, then there are N combinations ($C = N$) in this case. Suppose AP_1 is the one that is covered, then the probability for this condition is given from the concept of probability theory

$$Prob_1 = p_1(1-p_2)(1-p_3)\cdots(1-p_N) \tag{5.15}$$

Where $Pron_1$ is the probability that only AP_1 is covered while others are not. Note that we should skip the situation when all the APs are not covered. In this condition, no location estimation can be made, since no information can be used to determine the location of the receiver. Therefore, it is useless to discuss this situation.

Similarly, we can calculate the probabilities for all the other conditions ($Prob_2, Prob_3, \cdots, Prob_N$). Then the total CRLB can be calculated as follow

$$CRLB_{total} = \sum_{i=1}^{N} CRLB_i \cdot Prob_i \tag{5.16}$$

In this way, we can calculate the total CRLB no matter how many APs are covered.

5.4.3 3D CRLB Concerning Coverage Certainty

In the previous sections, all we have discussed are focused on the analysis in 2D condition. But in reality, 3D geolocation schemes are more important in indoor environment. Therefore, we should have a deeper look at how to expand our methods to 3D environment.

The empirical path loss model is no longer fit for 3D environment. In multistory building, the power-distance gradient α will change according to different distances, so the commonly used path loss model is given:

$$L_p = L_0 + \begin{cases} 20log_{10}r, & (10 \geq r \geq 1m) \\ 20 + 30log_{10}\dfrac{r}{10}, & (20 \geq r > 10m) \\ 29 + 60log_{10}\dfrac{r}{20}, & (40 \geq r > 20m) \\ 47 + 120log_{10}\dfrac{r}{40}, & (r > 40m) \end{cases} \tag{5.17}$$

From Equation (5.17), it is clear that path loss becomes greater when the distance between the transmitter and receiver becomes larger. But the method that we use to calculate coverage certainty stay the same. Equation (5.3) can still be used in 3D scenarios and the only difference is that we should replace the empirical path loss model with the 3D distance-partitioned model, which creates a different L_p.

The calculation for CRLB needs more expansion since the coordinate of every location becomes three dimensional. In 3D environment, we use similar method to start the derivation of CRLB.

To analyze the relation between RSS and the least location error (CRLB), we can apply partial differential to Equation (4.1) [8, 9]. Then we have

$$dP_i(x, y, z) = -\frac{10\alpha}{ln10}(\frac{x - x_i}{r_i^2}dx + \frac{y - y_i}{r_i^2}dy + \frac{z - z_i}{r_i^2}dz) \tag{5.18}$$

In this case, the matrix form should also be expanded to three dimension, where

$$d\boldsymbol{r} = \begin{bmatrix} dx \\ dy \\ dz \end{bmatrix}, \boldsymbol{H} = \begin{bmatrix} \frac{10\alpha_1}{ln10}\frac{x-x_1}{r_1^2} & \frac{10\alpha_1}{ln10}\frac{y-y_1}{r_1^2} & \frac{10\alpha_1}{ln10}\frac{z-z_1}{r_1^2} \\ \frac{10\alpha_2}{ln10}\frac{x-x_2}{r_2^2} & \frac{10\alpha_2}{ln10}\frac{y-y_2}{r_2^2} & \frac{10\alpha_2}{ln10}\frac{z-z_2}{r_2^2} \\ \vdots & \vdots & \vdots \\ \frac{10\alpha_N}{ln10}\frac{x-x_N}{r_N^2} & \frac{10\alpha_N}{ln10}\frac{y-y_N}{r_N^2} & \frac{10\alpha_N}{ln10}\frac{z-z_N}{r_N^2} \end{bmatrix}$$

By using the same least-square estimation method we mentioned before, estimation of the location error can be evaluated:

$$d\boldsymbol{r} = (\boldsymbol{H}'\boldsymbol{H})^{-1}\boldsymbol{H}'d\boldsymbol{P} \tag{5.19}$$

and the covariance matrix of the location error is

$$cov(d\boldsymbol{r}) = \sigma^2(\boldsymbol{H}'\boldsymbol{H}) = \begin{bmatrix} \sigma_x^2 & \sigma_{xy}^2 & \sigma_{xz}^2 \\ \sigma_{xy}^2 & \sigma_y^2 & \sigma_{yz}^2 \\ \sigma_{xz}^2 & \sigma_{yz}^2 & \sigma_z^2 \end{bmatrix} \tag{5.20}$$

Then the CRLB can be calculated as follow:

$$\sigma_r = \sqrt{\sigma_x^2 + \sigma_y^2 + \sigma_z^2} \tag{5.21}$$

Since every coverage probability and CRLB is redefined here, the 3D CRLB can be calculated in the same way which is described in Equation (5.16).

5.5 Results and Analysis

5.5.1 Effect of 2D AP Deployment

In this section, we evaluate the impact of different AP deployment on localization accuracy. From Equation (5.1) and designed scenarios for 2D localization, we can calculate the path loss for all the locations in these scenarios, which is depicted in Figure 5.1 And we can calculate the corresponding coverage probability

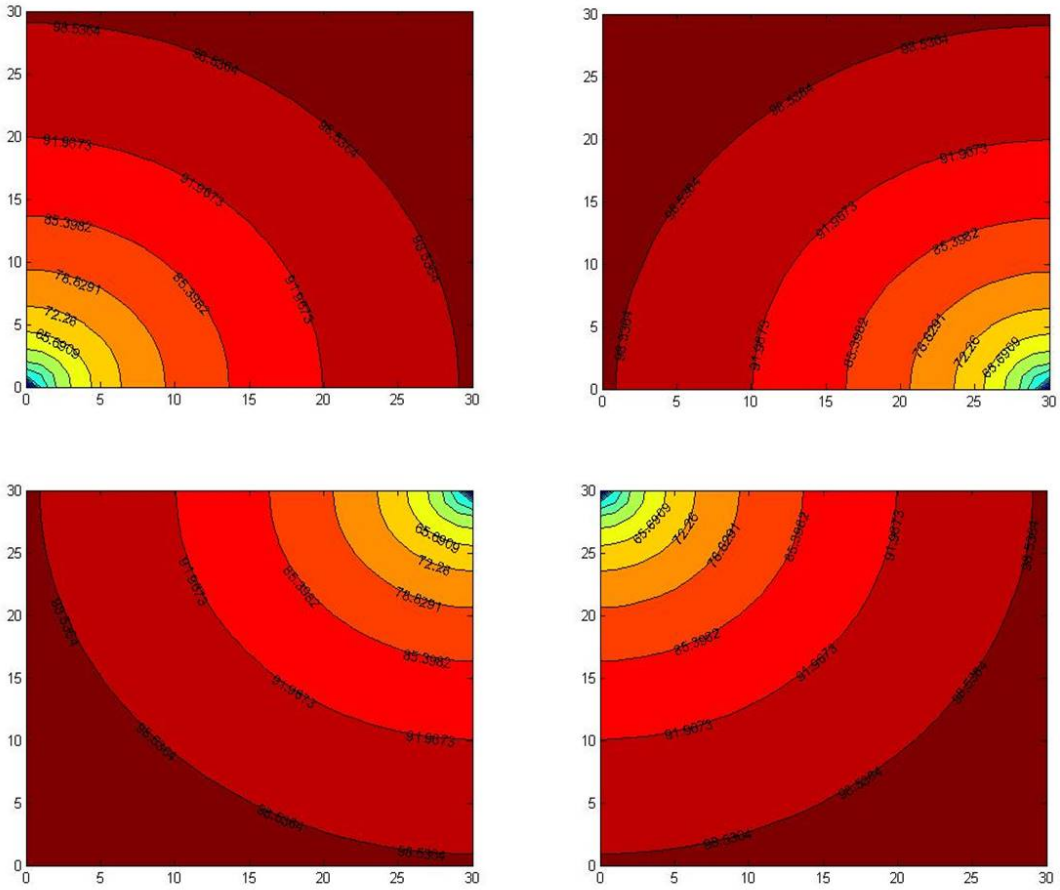

Figure 5.1: Path Loss from 4 APs in 2D Scenarios

by applying Equation (5.4), which is shown as follow.

We can also calculate CRLB for the 2D Scenarios and by applying Equation. Contours of the three scenarios are shown in Figure 5.2, 5.3 and 5.4. From these

figures, we can see that different types of deployment affect the localization accuracy in different patterns. CDFs for the three scenarios are given in Figure 5.5. It is obvious that, location accuracy improves as more APs are used. Error range of these three scenarios are shown in Table.

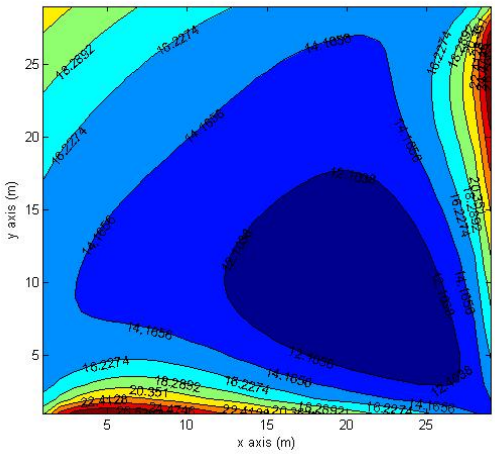

Figure 5.2: Contour for Scenario 1

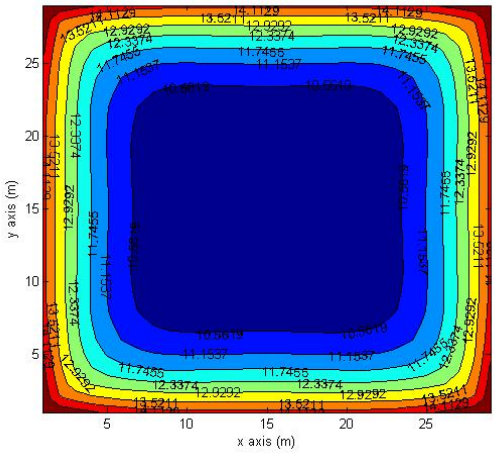

Figure 5.3: Contour for Scenario 2

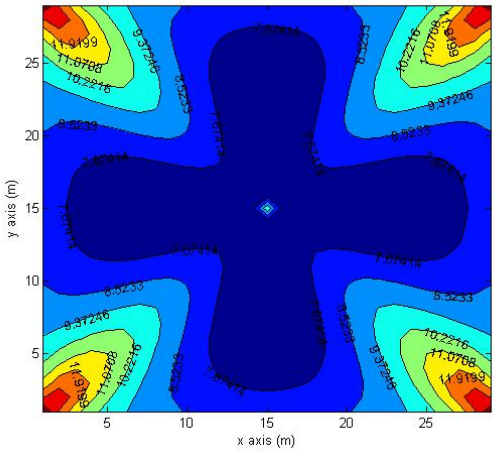

Figure 5.4: Contour for Scenario 3

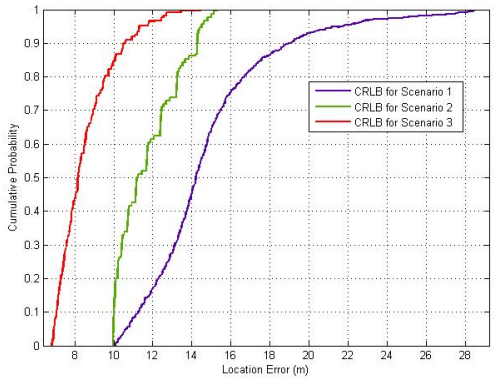

Figure 5.5: CDFs for 3 Scenarios in 2D

5.5.2 Effect of 3D AP Deployment

In 3D scenarios, if APs are deployed in a multistory building, the height of every story should be also considered when we are calculating the distance from the transmitter and the receiver.

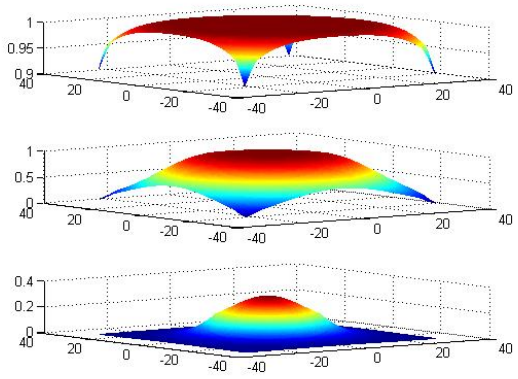

Figure 5.6: Coverage in 3D Scenarios

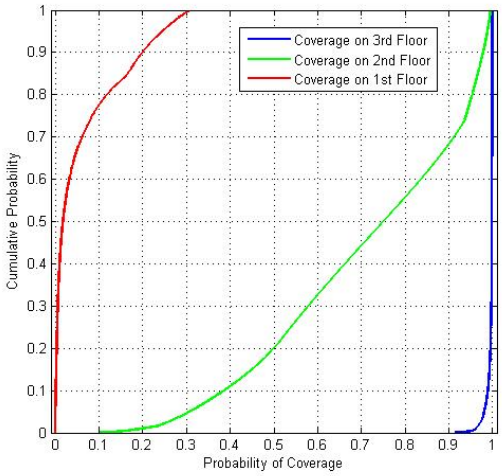

Figure 5.7: CDF of Coverage in 3D Scenarios

Chapter 6

Conclusion and Future Work

In this thesis, we present an approach to make intruder detection by analyzing GPS data and make multi-floor detection by using barometer in smart devices. We design scenarios on different floors in Atwater Kent laboratory and conduct series of experiments to collect data. By relating the estimation error with the LOA satellite number, it shows that estimation becomes more accurate as the LOS satellite number becomes greater. Based on the pressure-height physical law, we take the first derivative of the barometer and use pressure variance to detect floor transition. The handover algorithms are used to automatically detect intruder and multi-floor transition, and the experiment show that the algorithm performs well in indoor building and for any type of transport modes(stairs and elevators). To precisely identify which floor, we also consider noise, device bias and time difference in our pressure-height model.

We also present an approach to improve the performance of a 3D RSS-based geolocation system by using barometer in smart devices. A modified 3D path loss model is presented which brings penalty of ceilings into consideration. Based on the pressure-height physical law, we characterize the vertical estimation and fit it into a

Gaussian Distribution. Calculation of 3D CRLB is provided as an expansion of the original 2D CRLB for performance evaluation. Moreover, We design 3 scenarios of different floors with various AP deployment strategies and conduct series of experiments for comparison. The improvement is specified with contour and CDFs of the scenarios and quantified from a comparison table.

Future work includes: To expand our system to other kind of building, such as hospital, shopping mall, airport, and develop a more general solution. Fully combining the intruder detection, floor transition detection and floor identification technique, and try to provide a continuous indoor map selection system. Refine our pressure-height model, and bring up a precise time difference model. Integrate our technique into 2D indoor localization system to provide 3D localization. To expand our system to buildings with more complicated architecture, which will make the research more related to the real world. Fully combining the barometer and RSS signal should also be explored, so that smaller error can be reached. It is also feasible if we integrate our technique with other sensors in smart phones to find if more improvement can be reached.

Chapter 7

Appendix

7.1 Selected Matlab Code

```
clear all;close all;
%% basic path loss model
alpha1=4; % power gridiant
lpmax=108; % max path loss in dB
sigma1=8; % standard deviation of shadow fading
f=2.4e9; % transmitting frequency
c=3e8; % speed of light
lamda=c/f; % wave length
l0=40; % 1st meter path loss
pace=1;
x1=0;y1=0;
x2=0;y2=30;
x3=30;y3=30;
x4=30;y4=0;
```

```
x=0:pace:30;y=0:pace:30;
l1=length(x)-2;
r1=zeros(l1,l1);
r2=zeros(l1,l1);
r3=zeros(l1,l1);
for i=1:1:l1
    for j=1:1:l1
        r1(i,j)=sqrt((x(i+1)-x1)^2+(y(j+1)-y1)^2);
        r2(i,j)=sqrt((x(i+1)-x2)^2+(y(j+1)-y2)^2);
        r3(i,j)=sqrt((x(i+1)-x3)^2+(y(j+1)-y3)^2);
    end
end
lp1=l0+max(10*alpha1*log10(r1),-l0);
lp2=l0+max(10*alpha1*log10(r2),-l0);
lp3=l0+max(10*alpha1*log10(r3),-l0);
pc1=1-0.5*erfc((lpmax-lp1)/sqrt(2)/sigma1);
pc2=1-0.5*erfc((lpmax-lp2)/sqrt(2)/sigma1);
pc3=1-0.5*erfc((lpmax-lp3)/sqrt(2)/sigma1);
%% Coverage Probability
% 0 AP is covered
p0=(1-pc1).*(1-pc2).*(1-pc3);
% 1 access point is covered
p11=pc1.*(1-pc2).*(1-pc3);
p12=pc2.*(1-pc1).*(1-pc3);
p13=pc3.*(1-pc1).*(1-pc2);
p1=p11+p12+p13;
```

```
% 2 access points are covered
p21=pc1.*pc2.*(1-pc3);
p22=pc2.*pc3.*(1-pc1);
p23=pc1.*pc3.*(1-pc2);
p2=p21+p22+p23;
% 3 access points are covered
p3=pc1.*pc2.*pc3;
pcheck=p0+p1+p2+p3;

%% Cramer Rao Lower Bound for 2 APs
CRLB21=zeros(l1,l1);
CRLB22=zeros(l1,l1);
for i=1:1:l1
    for j=1:1:l1
        H21=[(x(i+1)-x1)/r1(i,j)^2,(y(j+1)-y1)/r1(i,j)^2;
            (x(i+1)-x2)/r2(i,j)^2,(y(j+1)-y2)/r2(i,j)^2]*(-alpha1*10/(log
        H22=[(x(i+1)-x2)/r2(i,j)^2,(y(j+1)-y2)/r2(i,j)^2;
            (x(i+1)-x3)/r3(i,j)^2,(y(j+1)-y3)/r3(i,j)^2]*(-alpha1*10/(log
        covr21=(sigma1^2)*(H21'*H21)^-1;
        covr22=(sigma1^2)*(H22'*H22)^-1;
        CRLB21(i,j)=sqrt(covr21(1,1)+covr21(2,2));
        CRLB22(i,j)=sqrt(covr22(1,1)+covr22(2,2));
    end
end
CRLB2=(CRLB21+CRLB22).*pace./2;
% figure(1)
```

```
% [C,h]=contourf(x(2:l1+1),y(2:l1+1),CRLB21,8);
% clabel(C,h);
%% Cramer Rao Lower Bound for 4 APs
CRLB3=zeros(l1,l1);
for i=1:1:l1
    for j=1:1:l1
        H31=[(x(i+1)-x1)/r1(i,j)^2,(y(j+1)-y1)/r1(i,j)^2;
             (x(i+1)-x2)/r2(i,j)^2,(y(j+1)-y2)/r2(i,j)^2;
             (x(i+1)-x3)/r3(i,j)^2,(y(j+1)-y3)/r3(i,j)^2]*(-alpha1*10/(log
        covr31=sigma1^2*(H31'*H31)^-1;
        CRLB3(i,j)=sqrt(covr31(1,1)+covr31(2,2));
    end
end
% figure(2)
% [C,h]=contourf(x(2:l1+1),y(2:l1+1),CRLB3,8);
% clabel(C,h);
CRLB_total_3=CRLB2.*p2+CRLB3.*p3;
figure(1)
[C,h]=contourf(x(2:l1+1),y(2:l1+1),CRLB_total_3,8);
clabel(C,h);
CRLB_total_3_re=reshape(CRLB_total_3,1,l1*l1);
%% Four
%% basic path loss model
alpha1=4; % power gridiant
lpmax=108; % max path loss in dB
sigma1=8; % standard deviation of shadow fading
```

```
f=2.4e9; % transmitting frequency
c=3e8; % speed of light
lamda=c/f; % wave length
l0=40; % 1st meter path loss
x1=0;y1=0;
x2=0;y2=30;
x3=30;y3=30;
x4=30;y4=0;
x=0:pace:30;y=0:pace:30;
l1=length(x)-2;
r1=zeros(l1,l1);
r2=zeros(l1,l1);
r3=zeros(l1,l1);
r4=zeros(l1,l1);
for i=1:1:l1
    for j=1:1:l1
        r1(i,j)=sqrt((x(i+1)-x1)^2+(y(j+1)-y1)^2);
        r2(i,j)=sqrt((x(i+1)-x2)^2+(y(j+1)-y2)^2);
        r3(i,j)=sqrt((x(i+1)-x3)^2+(y(j+1)-y3)^2);
        r4(i,j)=sqrt((x(i+1)-x4)^2+(y(j+1)-y4)^2);
    end
end
lp1=l0+max(10*alpha1*log10(r1),-l0);
lp2=l0+max(10*alpha1*log10(r2),-l0);
lp3=l0+max(10*alpha1*log10(r3),-l0);
lp4=l0+max(10*alpha1*log10(r4),-l0);
```

```
pc1=1-0.5*erfc((lpmax-lp1)/sqrt(2)/sigma1);
pc2=1-0.5*erfc((lpmax-lp2)/sqrt(2)/sigma1);
pc3=1-0.5*erfc((lpmax-lp3)/sqrt(2)/sigma1);
pc4=1-0.5*erfc((lpmax-lp4)/sqrt(2)/sigma1);
%% Coverage Probability
% 0 AP is covered
p0=(1-pc1).*(1-pc2).*(1-pc3).*(1-pc4);
% 1 access point is covered
p11=pc1.*(1-pc2).*(1-pc3).*(1-pc4);
p12=pc2.*(1-pc1).*(1-pc3).*(1-pc4);
p13=pc3.*(1-pc1).*(1-pc2).*(1-pc4);
p14=pc4.*(1-pc1).*(1-pc2).*(1-pc3);
p1=p11+p12+p13+p14;
% 2 access points are covered
p21=pc1.*pc2.*(1-pc3).*(1-pc4);
p22=pc1.*pc3.*(1-pc2).*(1-pc4);
p23=pc1.*pc4.*(1-pc2).*(1-pc3);
p24=pc2.*pc3.*(1-pc1).*(1-pc4);
p25=pc2.*pc4.*(1-pc1).*(1-pc3);
p26=pc3.*pc4.*(1-pc1).*(1-pc2);
p2=p21+p22+p23+p24+p25+p26;
% 3 access points are covered
p34=pc1.*pc2.*pc3.*(1-pc4);
p33=pc1.*pc2.*pc4.*(1-pc3);
p32=pc1.*pc3.*pc4.*(1-pc2);
p31=pc2.*pc3.*pc4.*(1-pc1);
```

```
p3=p31+p32+p33+p34;
% 4 access points are covered
p4=pc1.*pc2.*pc3.*pc4;

%% Cramer Rao Lower Bound for 1 AP
% CRLB11=(log(10)*sigma1/(10*alpha1))*r1;
% CRLB12=log(10)*sigma1/(10*alpha1)*r2;
% CRLB13=log(10)*sigma1/(10*alpha1)*r3;;
% CRLB14=log(10)*sigma1/(10*alpha1)*r4;
% CRLB1=(CRLB11+CRLB12+CRLB13+CRLB14)./4;
% figure(1)
% [C,h]=contourf(x(2:l1+1),y(2:l1+1),CRLB1,8);
% clabel(C,h);

%% Cramer Rao Lower Bound for 2 APs
CRLB21=zeros(l1,l1);
CRLB22=zeros(l1,l1);
CRLB23=zeros(l1,l1);
CRLB24=zeros(l1,l1);
for i=1:1:l1
    for j=1:1:l1
        H21=[(x(i+1)-x1)/r1(i,j)^2,(y(j+1)-y1)/r1(i,j)^2;
            (x(i+1)-x2)/r2(i,j)^2,(y(j+1)-y2)/r2(i,j)^2]*(-alpha1*10/(log
        H22=[(x(i+1)-x1)/r1(i,j)^2,(y(j+1)-y1)/r1(i,j)^2;
            (x(i+1)-x4)/r4(i,j)^2,(y(j+1)-y4)/r4(i,j)^2]*(-alpha1*10/(log
        H23=[(x(i+1)-x2)/r2(i,j)^2,(y(j+1)-y2)/r2(i,j)^2;
```

```
            (x(i+1)-x3)/r3(i,j)^2,(y(j+1)-y3)/r3(i,j)^2]*(-alpha1*10/(log
        H24=[(x(i+1)-x3)/r3(i,j)^2,(y(j+1)-y3)/r3(i,j)^2;
            (x(i+1)-x4)/r4(i,j)^2,(y(j+1)-y4)/r4(i,j)^2]*(-alpha1*10/(log
        covr21=(sigma1^2)*(H21'*H21)^-1;
        covr22=(sigma1^2)*(H22'*H22)^-1;
        covr23=(sigma1^2)*(H23'*H23)^-1;
        covr24=(sigma1^2)*(H24'*H24)^-1;
        CRLB21(i,j)=sqrt(covr21(1,1)+covr21(2,2));
        CRLB22(i,j)=sqrt(covr22(1,1)+covr22(2,2));
        CRLB23(i,j)=sqrt(covr23(1,1)+covr23(2,2));
        CRLB24(i,j)=sqrt(covr24(1,1)+covr24(2,2));
    end
end
CRLB2=(CRLB21+CRLB22+CRLB23+CRLB24).*pace./4;
% figure(1)
% [C,h]=contourf(x(2:l1+1),y(2:l1+1),CRLB21,8);
% clabel(C,h);
%% Cramer Rao Lower Bound for 3 APs
CRLB31=zeros(l1,l1);
CRLB32=zeros(l1,l1);
CRLB33=zeros(l1,l1);
CRLB34=zeros(l1,l1);
for i=1:1:l1
    for j=1:1:l1
        H31=[(x(i+1)-x2)/r2(i,j)^2,(y(j+1)-y2)/r2(i,j)^2;
            (x(i+1)-x3)/r3(i,j)^2,(y(j+1)-y3)/r3(i,j)^2;
```

```
            (x(i+1)-x4)/r4(i,j)^2,(y(j+1)-y4)/r4(i,j)^2]*(-alpha1*10/(log
        H32=[(x(i+1)-x1)/r1(i,j)^2,(y(j+1)-y1)/r1(i,j)^2;
            (x(i+1)-x3)/r3(i,j)^2,(y(j+1)-y3)/r3(i,j)^2;
            (x(i+1)-x4)/r4(i,j)^2,(y(j+1)-y4)/r4(i,j)^2]*(-alpha1*10/(log
        H33=[(x(i+1)-x1)/r1(i,j)^2,(y(j+1)-y1)/r1(i,j)^2;
            (x(i+1)-x2)/r2(i,j)^2,(y(j+1)-y2)/r2(i,j)^2;
            (x(i+1)-x4)/r4(i,j)^2,(y(j+1)-y4)/r4(i,j)^2]*(-alpha1*10/(log
        H34=[(x(i+1)-x1)/r1(i,j)^2,(y(j+1)-y1)/r1(i,j)^2;
            (x(i+1)-x2)/r2(i,j)^2,(y(j+1)-y2)/r2(i,j)^2;
            (x(i+1)-x3)/r3(i,j)^2,(y(j+1)-y3)/r3(i,j)^2]*(-alpha1*10/(log
        covr31=sigma1^2*(H31'*H31)^-1;
        covr32=sigma1^2*(H32'*H32)^-1;
        covr33=sigma1^2*(H33'*H33)^-1;
        covr34=sigma1^2*(H34'*H34)^-1;
        CRLB31(i,j)=sqrt(covr31(1,1)+covr31(2,2));
        CRLB32(i,j)=sqrt(covr32(1,1)+covr32(2,2));
        CRLB33(i,j)=sqrt(covr33(1,1)+covr33(2,2));
        CRLB34(i,j)=sqrt(covr34(1,1)+covr34(2,2));
    end
end
CRLB3=(CRLB31+CRLB32+CRLB33+CRLB34)./4;
% figure(2)
% [C,h]=contourf(x(2:l1+1),y(2:l1+1),CRLB3,8);
% clabel(C,h);
%% Cramer Rao Lower Bound for 4 APs
CRLB4=zeros(l1,l1);
```

```
for i=1:1:l1
    for j=1:1:l1
        H4=[(x(i+1)-x1)/r1(i,j)^2,(y(j+1)-y1)/r1(i,j)^2;
            (x(i+1)-x2)/r2(i,j)^2,(y(j+1)-y2)/r2(i,j)^2;
            (x(i+1)-x3)/r3(i,j)^2,(y(j+1)-y3)/r3(i,j)^2;
            (x(i+1)-x4)/r4(i,j)^2,(y(j+1)-y4)/r4(i,j)^2]*(-alpha1*10/(log(
        covr4=sigma1^2*(H4'*H4)^-1;
        CRLB4(i,j)=sqrt(covr4(1,1)+covr4(2,2));
    end
end
% figure(3)
% [C,h]=contourf(x(2:l1+1),y(2:l1+1),CRLB4,8);
% clabel(C,h);
CRLB_total_4=CRLB2.*p2+CRLB3.*p3+CRLB4.*p4;
figure(2)
[C,h]=contourf(x(2:l1+1),y(2:l1+1),CRLB_total_4,8);
clabel(C,h);
CRLB_total_4_re=reshape(CRLB_total_4,1,l1*l1);
%% Five
%% basic path loss model
alpha1=4; % power gridiant
lpmax=108; % max path loss in dB
sigma1=8; % standard deviation of shadow fading
f=2.4e9; % transmitting frequency
c=3e8; % speed of light
lamda=c/f; % wave length
```

```
l0=40; % 1st meter path loss
x1=0;y1=0;
x2=0;y2=30;
x3=30;y3=30;
x4=30;y4=0;
x5=15;y5=15;
x=0:pace:30;y=0:pace:30;
l1=length(x)-2;
r1=zeros(l1,l1);
r2=zeros(l1,l1);
r3=zeros(l1,l1);
r4=zeros(l1,l1);
r5=zeros(l1,l1);
for i=1:1:l1
    for j=1:1:l1
        r1(i,j)=sqrt((x(i+1)-x1)^2+(y(j+1)-y1)^2);
        r2(i,j)=sqrt((x(i+1)-x2)^2+(y(j+1)-y2)^2);
        r3(i,j)=sqrt((x(i+1)-x3)^2+(y(j+1)-y3)^2);
        r4(i,j)=sqrt((x(i+1)-x4)^2+(y(j+1)-y4)^2);
        r5(i,j)=sqrt((x(i+1)-x5)^2+(y(j+1)-y5)^2);
        if r5(i,j)==0
            r5(i,j)=1;
        end
    end
end
lp1=l0+max(10*alpha1*log10(r1),-l0);
```

```
lp2=l0+max(10*alpha1*log10(r2),-l0);
lp3=l0+max(10*alpha1*log10(r3),-l0);
lp4=l0+max(10*alpha1*log10(r4),-l0);
lp5=l0+max(10*alpha1*log10(r5),-l0);
pc1=1-0.5*erfc((lpmax-lp1)/sqrt(2)/sigma1);
pc2=1-0.5*erfc((lpmax-lp2)/sqrt(2)/sigma1);
pc3=1-0.5*erfc((lpmax-lp3)/sqrt(2)/sigma1);
pc4=1-0.5*erfc((lpmax-lp4)/sqrt(2)/sigma1);
pc5=1-0.5*erfc((lpmax-lp5)/sqrt(2)/sigma1);
%% Coverage Probability
% 0 AP is covered
p0=(1-pc1).*(1-pc2).*(1-pc3).*(1-pc4).*(1-pc5);
% 1 access point is covered
p11=pc1.*(1-pc2).*(1-pc3).*(1-pc4).*(1-pc5);
p12=pc2.*(1-pc1).*(1-pc3).*(1-pc4).*(1-pc5);
p13=pc3.*(1-pc1).*(1-pc2).*(1-pc4).*(1-pc5);
p14=pc4.*(1-pc1).*(1-pc2).*(1-pc3).*(1-pc5);
p15=pc5.*(1-pc1).*(1-pc2).*(1-pc3).*(1-pc4);
p1=p11+p12+p13+p14+p15;
% 2 access points are covered
p21=pc1.*pc2.*(1-pc3).*(1-pc4).*(1-pc5);
p22=pc1.*pc3.*(1-pc2).*(1-pc4).*(1-pc5);
p23=pc1.*pc4.*(1-pc2).*(1-pc3).*(1-pc5);
p24=pc1.*pc5.*(1-pc2).*(1-pc3).*(1-pc4);
p25=pc2.*pc3.*(1-pc1).*(1-pc4).*(1-pc5);
p26=pc2.*pc4.*(1-pc1).*(1-pc3).*(1-pc5);
```

```
p27=pc2.*pc5.*(1-pc1).*(1-pc3).*(1-pc4);
p28=pc3.*pc4.*(1-pc1).*(1-pc2).*(1-pc5);
p29=pc3.*pc5.*(1-pc1).*(1-pc2).*(1-pc4);
p210=pc4.*pc5.*(1-pc1).*(1-pc2).*(1-pc3);
p2=p21+p22+p23+p24+p25+p26+p27+p28+p29+p210;
% 3 access points are covered
p31=pc1.*pc2.*pc3.*(1-pc4).*(1-pc5);
p32=pc1.*pc2.*pc4.*(1-pc3).*(1-pc5);
p33=pc1.*pc2.*pc5.*(1-pc3).*(1-pc4);
p34=pc1.*pc3.*pc4.*(1-pc2).*(1-pc5);
p35=pc1.*pc3.*pc5.*(1-pc2).*(1-pc4);
p36=pc1.*pc4.*pc5.*(1-pc2).*(1-pc3);
p37=pc2.*pc3.*pc4.*(1-pc1).*(1-pc5);
p38=pc2.*pc3.*pc5.*(1-pc1).*(1-pc4);
p39=pc2.*pc4.*pc5.*(1-pc1).*(1-pc3);
p310=pc3.*pc4.*pc5.*(1-pc1).*(1-pc2);
p3=p31+p32+p33+p34+p35+p36+p37+p38+p39+p310;
% 4 access points are covered
p41=pc2.*pc3.*pc4.*pc5.*(1-pc1);
p42=pc1.*pc3.*pc4.*pc5.*(1-pc2);
p43=pc1.*pc2.*pc4.*pc5.*(1-pc3);
p44=pc1.*pc2.*pc3.*pc5.*(1-pc4);
p45=pc1.*pc2.*pc3.*pc4.*(1-pc5);
p4=p41+p42+p43+p44+p45;
% 5 access points are covered
p5=pc1.*pc2.*pc3.*pc4.*pc5;
```

```
pcheck=p0+p1+p2+p3+p4+p5;

%% Cramer Rao Lower Bound for 1 AP
% CRLB11=(log(10)*sigma1/(10*alpha1))*r1;
% CRLB12=log(10)*sigma1/(10*alpha1)*r2;
% CRLB13=log(10)*sigma1/(10*alpha1)*r3;;
% CRLB14=log(10)*sigma1/(10*alpha1)*r4;
% CRLB1=(CRLB11+CRLB12+CRLB13+CRLB14)./4;
% figure(1)
% [C,h]=contourf(x(2:l1+1),y(2:l1+1),CRLB1,8);
% clabel(C,h);

%% Cramer Rao Lower Bound for 2 APs
CRLB21=zeros(l1,l1);
CRLB23=zeros(l1,l1);
CRLB25=zeros(l1,l1);
CRLB28=zeros(l1,l1);
for i=1:1:l1
    for j=1:1:l1
        H21=[(x(i+1)-x1)/r1(i,j)^2,(y(j+1)-y1)/r1(i,j)^2;
             (x(i+1)-x2)/r2(i,j)^2,(y(j+1)-y2)/r2(i,j)^2]*(-alpha1*10/(log
        H23=[(x(i+1)-x1)/r1(i,j)^2,(y(j+1)-y1)/r1(i,j)^2;
             (x(i+1)-x4)/r4(i,j)^2,(y(j+1)-y4)/r4(i,j)^2]*(-alpha1*10/(log
        H25=[(x(i+1)-x2)/r2(i,j)^2,(y(j+1)-y2)/r2(i,j)^2;
             (x(i+1)-x3)/r3(i,j)^2,(y(j+1)-y3)/r3(i,j)^2]*(-alpha1*10/(log
        H28=[(x(i+1)-x3)/r3(i,j)^2,(y(j+1)-y3)/r3(i,j)^2;
```

```
            (x(i+1)-x4)/r4(i,j)^2,(y(j+1)-y4)/r4(i,j)^2]*(-alpha1*10/(log
        covr21=(sigma1^2)*(H21'*H21)^-1;
        covr23=(sigma1^2)*(H23'*H23)^-1;
        covr25=(sigma1^2)*(H25'*H25)^-1;
        covr28=(sigma1^2)*(H28'*H28)^-1;
        CRLB21(i,j)=sqrt(covr21(1,1)+covr21(2,2));
        CRLB23(i,j)=sqrt(covr23(1,1)+covr23(2,2));
        CRLB25(i,j)=sqrt(covr25(1,1)+covr25(2,2));
        CRLB28(i,j)=sqrt(covr28(1,1)+covr28(2,2));
    end
end
CRLB2=(CRLB21+CRLB23+CRLB25+CRLB28).*pace./4;
% figure(1)
% [C,h]=contourf(x(2:l1+1),y(2:l1+1),CRLB2,8);
% clabel(C,h);
%% Cramer Rao Lower Bound for 3 APs
CRLB31=zeros(l1,l1);
CRLB32=zeros(l1,l1);
CRLB33=zeros(l1,l1);
CRLB34=zeros(l1,l1);
CRLB36=zeros(l1,l1);
CRLB37=zeros(l1,l1);
CRLB38=zeros(l1,l1);
CRLB310=zeros(l1,l1);
for i=1:1:l1
    for j=1:1:l1
```

```
H31=[(x(i+1)-x1)/r1(i,j)^2,(y(j+1)-y1)/r1(i,j)^2;
     (x(i+1)-x2)/r2(i,j)^2,(y(j+1)-y2)/r2(i,j)^2;
     (x(i+1)-x3)/r3(i,j)^2,(y(j+1)-y3)/r3(i,j)^2]*(-alpha1*10/(log
H32=[(x(i+1)-x1)/r1(i,j)^2,(y(j+1)-y1)/r1(i,j)^2;
     (x(i+1)-x2)/r2(i,j)^2,(y(j+1)-y2)/r2(i,j)^2;
     (x(i+1)-x4)/r4(i,j)^2,(y(j+1)-y4)/r4(i,j)^2]*(-alpha1*10/(log
H33=[(x(i+1)-x1)/r1(i,j)^2,(y(j+1)-y1)/r1(i,j)^2;
     (x(i+1)-x2)/r2(i,j)^2,(y(j+1)-y2)/r2(i,j)^2;
     (x(i+1)-x5)/r5(i,j)^2,(y(j+1)-y5)/r5(i,j)^2]*(-alpha1*10/(log
H34=[(x(i+1)-x1)/r1(i,j)^2,(y(j+1)-y1)/r1(i,j)^2;
     (x(i+1)-x3)/r3(i,j)^2,(y(j+1)-y3)/r3(i,j)^2;
     (x(i+1)-x4)/r4(i,j)^2,(y(j+1)-y4)/r4(i,j)^2]*(-alpha1*10/(log
H36=[(x(i+1)-x1)/r1(i,j)^2,(y(j+1)-y1)/r1(i,j)^2;
     (x(i+1)-x4)/r4(i,j)^2,(y(j+1)-y4)/r4(i,j)^2;
     (x(i+1)-x5)/r5(i,j)^2,(y(j+1)-y5)/r5(i,j)^2]*(-alpha1*10/(log
H37=[(x(i+1)-x2)/r2(i,j)^2,(y(j+1)-y2)/r2(i,j)^2;
     (x(i+1)-x3)/r3(i,j)^2,(y(j+1)-y3)/r3(i,j)^2;
     (x(i+1)-x4)/r4(i,j)^2,(y(j+1)-y4)/r4(i,j)^2]*(-alpha1*10/(log
H38=[(x(i+1)-x2)/r2(i,j)^2,(y(j+1)-y2)/r2(i,j)^2;
     (x(i+1)-x3)/r3(i,j)^2,(y(j+1)-y3)/r3(i,j)^2;
     (x(i+1)-x5)/r5(i,j)^2,(y(j+1)-y5)/r5(i,j)^2]*(-alpha1*10/(log
H310=[(x(i+1)-x3)/r3(i,j)^2,(y(j+1)-y3)/r3(i,j)^2;
     (x(i+1)-x4)/r4(i,j)^2,(y(j+1)-y4)/r4(i,j)^2;
     (x(i+1)-x5)/r5(i,j)^2,(y(j+1)-y5)/r5(i,j)^2]*(-alpha1*10/(log
covr31=sigma1^2*(H31'*H31)^-1;
covr32=sigma1^2*(H32'*H32)^-1;
```

```
            covr33=sigma1^2*(H33'*H33)^-1;
            covr34=sigma1^2*(H34'*H34)^-1;
            covr36=sigma1^2*(H36'*H36)^-1;
            covr37=sigma1^2*(H37'*H37)^-1;
            covr38=sigma1^2*(H38'*H38)^-1;
            covr310=sigma1^2*(H310'*H310)^-1;
            CRLB31(i,j)=sqrt(covr31(1,1)+covr31(2,2));
            CRLB32(i,j)=sqrt(covr32(1,1)+covr32(2,2));
            CRLB33(i,j)=sqrt(covr33(1,1)+covr33(2,2));
            CRLB34(i,j)=sqrt(covr34(1,1)+covr34(2,2));
            CRLB36(i,j)=sqrt(covr36(1,1)+covr36(2,2));
            CRLB37(i,j)=sqrt(covr37(1,1)+covr37(2,2));
            CRLB38(i,j)=sqrt(covr38(1,1)+covr38(2,2));
            CRLB310(i,j)=sqrt(covr310(1,1)+covr310(2,2));
        end
    end
    CRLB3=(CRLB31+CRLB32+CRLB33+CRLB34+CRLB36+CRLB37+CRLB38+CRLB310)./8;
    % figure(2)
    % [C,h]=contourf(x(2:l1+1),y(2:l1+1),CRLB3,8);
    % clabel(C,h);
    %% Cramer Rao Lower Bound for 4 APs
    CRLB41=zeros(l1,l1);
    CRLB42=zeros(l1,l1);
    CRLB43=zeros(l1,l1);
    CRLB44=zeros(l1,l1);
    CRLB45=zeros(l1,l1);
```

```
for i=1:1:l1
    for j=1:1:l1
        H41=[(x(i+1)-x2)/r2(i,j)^2,(y(j+1)-y2)/r2(i,j)^2;
            (x(i+1)-x3)/r3(i,j)^2,(y(j+1)-y3)/r3(i,j)^2;
            (x(i+1)-x4)/r4(i,j)^2,(y(j+1)-y4)/r4(i,j)^2
            (x(i+1)-x5)/r5(i,j)^2,(y(j+1)-y5)/r5(i,j)^2;]*(-alpha1*10/(log
        H42=[(x(i+1)-x1)/r1(i,j)^2,(y(j+1)-y1)/r1(i,j)^2;
            (x(i+1)-x3)/r3(i,j)^2,(y(j+1)-y3)/r3(i,j)^2;
            (x(i+1)-x4)/r4(i,j)^2,(y(j+1)-y4)/r4(i,j)^2;
            (x(i+1)-x5)/r5(i,j)^2,(y(j+1)-y5)/r5(i,j)^2]*(-alpha1*10/(log(
        H43=[(x(i+1)-x1)/r1(i,j)^2,(y(j+1)-y1)/r1(i,j)^2;
            (x(i+1)-x2)/r2(i,j)^2,(y(j+1)-y2)/r2(i,j)^2;
            (x(i+1)-x4)/r4(i,j)^2,(y(j+1)-y4)/r4(i,j)^2;
            (x(i+1)-x5)/r5(i,j)^2,(y(j+1)-y5)/r5(i,j)^2]*(-alpha1*10/(log(
        H44=[(x(i+1)-x1)/r1(i,j)^2,(y(j+1)-y1)/r1(i,j)^2;
            (x(i+1)-x2)/r2(i,j)^2,(y(j+1)-y2)/r2(i,j)^2;
            (x(i+1)-x3)/r3(i,j)^2,(y(j+1)-y3)/r3(i,j)^2;
            (x(i+1)-x5)/r5(i,j)^2,(y(j+1)-y5)/r5(i,j)^2]*(-alpha1*10/(log(
        H45=[(x(i+1)-x1)/r1(i,j)^2,(y(j+1)-y1)/r1(i,j)^2;
            (x(i+1)-x2)/r2(i,j)^2,(y(j+1)-y2)/r2(i,j)^2;
            (x(i+1)-x3)/r3(i,j)^2,(y(j+1)-y3)/r3(i,j)^2;
            (x(i+1)-x4)/r4(i,j)^2,(y(j+1)-y4)/r4(i,j)^2]*(-alpha1*10/(log(
        covr41=sigma1^2*(H41'*H41)^-1;
        covr42=sigma1^2*(H42'*H42)^-1;
        covr43=sigma1^2*(H43'*H43)^-1;
        covr44=sigma1^2*(H44'*H44)^-1;
```

```
        covr45=sigma1^2*(H45'*H45)^-1;
        CRLB41(i,j)=sqrt(covr41(1,1)+covr41(2,2));
        CRLB42(i,j)=sqrt(covr42(1,1)+covr42(2,2));
        CRLB43(i,j)=sqrt(covr43(1,1)+covr43(2,2));
        CRLB44(i,j)=sqrt(covr44(1,1)+covr44(2,2));
        CRLB45(i,j)=sqrt(covr45(1,1)+covr45(2,2));
    end
end
CRLB4=(CRLB41+CRLB42+CRLB43+CRLB44+CRLB45)./5;
% figure(3)
% [C,h]=contourf(x(2:l1+1),y(2:l1+1),CRLB4,8);
% clabel(C,h);
% CRLB_total=CRLB2+CRLB3+CRLB4;
% figure(4)
% [C,h]=contourf(x(2:l1+1),y(2:l1+1),CRLB_total,8);
% clabel(C,h);
%% Cramer Rao Lower Bound for 5 APs
CRLB5=zeros(l1,l1);
for i=1:1:l1
    for j=1:1:l1
        H5=[(x(i+1)-x1)/r1(i,j)^2,(y(j+1)-y1)/r1(i,j)^2;
            (x(i+1)-x2)/r2(i,j)^2,(y(j+1)-y2)/r2(i,j)^2;
            (x(i+1)-x3)/r3(i,j)^2,(y(j+1)-y3)/r3(i,j)^2;
            (x(i+1)-x4)/r4(i,j)^2,(y(j+1)-y4)/r4(i,j)^2;
            (x(i+1)-x5)/r5(i,j)^2,(y(j+1)-y5)/r5(i,j)^2]*(-alpha1*10/(log(
        covr5=sigma1^2*(H5'*H5)^-1;
```

```
            CRLB5(i,j)=sqrt(covr5(1,1)+covr5(2,2));
        end
    end
    CRLB_total_5=CRLB2.*p2+CRLB3.*p3+CRLB4.*p4+CRLB5.*p5;
    figure(3)
    [C,h]=contourf(x(2:l1+1),y(2:l1+1),CRLB_total_5,8);
    clabel(C,h);
    % CRLB_total=CRLB2+CRLB3+CRLB4;
    % figure(4)
    % [C,h]=contourf(x(2:l1+1),y(2:l1+1),CRLB_total,8);
    % clabel(C,h);
    CRLB_total_5_re=reshape(CRLB_total_5,1,l1*l1);
```

Bibliography

[1] Pahlavan, Kaveh, Xinrong Li, and J-P. Makela. "Indoor geolocation science and technology." Communications Magazine, IEEE 40.2 (2002): 112-118.

[2] He J, Geng Y, Pahlavan K. Toward Accurate Human Tracking: Modeling Time-of-Arrival for Wireless Wearable Sensors in Multipath Environment[J]. Sensors Journal, IEEE, 2014, 14(11): 3996-4006.

[3] He J, Geng Y, Liu F, et al. CC-KF: Enhanced TOA Performance in Multi-path and NLOS Indoor Extreme Environment[J]. Sensors Journal, IEEE, 2014, 14(11): 3766-3774.

[4] Iadanza E, Dori F, Miniati R, et al. Patients tracking and identifying inside hospital: A multilayer method to plan an RFId solution[C]//Engineering in Medicine and Biology Society, 2008. EMBS 2008. 30th Annual International Conference of the IEEE. IEEE, 2008: 1462-1465.

[5] Liu G, Geng Y, Pahlavan K. Effects of calibration RFID tags on performance of inertial navigation in indoor environment[C]//Computing, Networking and Communications (ICNC), 2015 International Conference on. IEEE, 2015: 945-949.

[6] Pahlavan K, Krishnamurthy P, Geng Y. Localization Challenges for the Emergence of the Smart World[J].

[7] Alemdar H, Ersoy C. Wireless sensor networks for healthcare: A survey[J]. Computer Networks, 2010, 54(15): 2688-2710.

[8] Li Z, Yang Y, Pahlavan K. Using iBeacon for In-Room Newborns Localization in Hospital//International Symposium on Medical Information and Communication Technology (ISMICT'16).

[9] Wang Y, Fu R, Ye Y, et al. Performance bounds for RF positioning of endoscopy camera capsules[C]//Biomedical Wireless Technologies, Networks, and Sensing Systems (BioWireleSS), 2011 IEEE Topical Conference on. IEEE, 2011: 71-74.

[10] Pahlavan K, Levesque A H. Wireless information networks[M]. John Wiley & Sons, 2005.

[11] Geng Y, Pahlavan K. Design, Implementation and Fundamental Limits of Image and RF Based Wireless Capsule Endoscopy Hybrid Localization[J]. 2015.

[12] Chen Y, Kobayashi H. Signal strength based indoor geolocation[C]//Communications, 2002. ICC 2002. IEEE International Conference on. IEEE, 2002, 1: 436-439.

[13] Julang Ying, Chao Ren and Kaveh Pahlavan, On Automated Map Selection Problem in Indoor Navigation for Smart Devices, The Workshop of IEEE 2015 Wireless Telecommunications Symposium (WTS), New York City, USA, April 15-17, 2015.

[14] Li S, Geng Y, He J, et al. Analysis of three-dimensional maximum likelihood algorithm for capsule endoscopy localization[C]//Biomedical Engineering and Informatics (BMEI), 2012 5th International Conference on. IEEE, 2012: 721-725.

[15] Pahlavan, Kaveh, Xinrong Li, and J-P. Makela. "Indoor geolocation science and technology." Communications Magazine, IEEE 40.2 (2002): 112-118.

[16] Y. Geng, J.He, H. Deng and K. Pahlavan, Modeling the Effect of Human Body on TOA Ranging for Indoor Human Tracking with Wrist Mounted Sensor, IEEE 16th International Conference on Wireless Personal Multimedia Communications (WPMC), Atlantic City, NJ, Jun. 2013

[17] W. Huang and Y.Geng, Identification Method of Attack Path Based on Immune Intrusion Detection, Journal of Networks, 9(4), 964-971, 2014

[18] G. Liu, Y. Geng and K. Pahlavan, Effects of Calibration RFID Tags on performance of Inertial Navigation in Indoor Environment, *IEEE International Conference on Computing, Networking and Communications (ICNC)*, Anaheim, CA, Feb. 2015

[19] Rantakokko, Jouni, et al. "Accurate and reliable soldier and first responder indoor positioning: multisensor systems and cooperative localization." Wireless Communications, IEEE 18.2 (2011): 10-18.

[20] Retscher, Gnther, and Michael Thienelt. "NAVIOA navigation and guidance service for pedestrians." Positioning 1.08 (2004).

[21] Hatami, Ahmad, and Kaveh Pahlavan. "In-building intruder detection for WLAN access." Position Location and Navigation Symposium, 2004. PLANS 2004. IEEE, 2004.

[22] Wang, Hui, et al. "Fusion of barometric sensors, WLAN signals and building information for 3-D indoor/campus localization." proceedings of International

Conference on Multisensor Fusion and Integration for Intelligent Systems (MFI 2006), S. 2006.

[23] Gilliron, Pierre-Yves, and Bertrand Merminod. "Personal navigation system for indoor applications." 11th IAIN World Congress. 2003.

[24] Kourogi, Masakatsu, et al. "Indoor/outdoor pedestrian navigation with an embedded GPS/RFID/self-contained sensor system." Advances in Artificial Reality and Tele-Existence. Springer Berlin Heidelberg, 2006. 1310-1321.

[25] Bird, Jeff, and Dale Arden. "Indoor navigation with foot-mounted strapdown inertial navigation and magnetic sensors [emerging opportunities for localization and tracking]." Wireless Communications, IEEE 18.2 (2011): 28-35.

[26] Inzerilli, Tiziano, et al. "A location-based vertical handover algorithm for limitation of the ping-pong effect." Networking and Communications, 2008. WIMOB'08. IEEE International Conference on Wireless and Mobile Computing,. IEEE, 2008.

[27] Yuzhang Zang, Kaveh Pahlavan, Yang Zheng, and Le Wang, "UWB Gesture Detection for Visually Impaired Remote Control, IEEE International Symposium on Medical Information and Communication Technology (ISMICT), Worcester, USA, March 21-23, 2016.

[28] Dan Liu, Yishuang Geng and Kaveh Pahlavan, "End-to-end Power Optimization in Non-Homogenous Relay Environment for Wireless Body Area Networks (WBANs), IEEE International Symposium on Medical Information and Communication Technology (ISMICT), Worcester, USA, March 21-23, 2016.

[29] Yang Yang, Zhouchi Li and Kaveh Pahlavan, "Using iBeacon for Intelligent In-Room Presence Detection, 2016 IEEE International Multi-Disciplinary Conference on Cognitive Methods in Situation Awareness and Decision Support (CogSIMA), San Diego, USA, March 21-25, 2016.

[30] Luyao Niu, Yingyue Fan, Kaveh Pahlavan, Guanxiong Liu and Yishuang Geng, "On the Accuracy of Wi-Fi Localization Using Robot and Human Collected Signatures, IEEE International Conference on Consumer Electronics (ICCE), Las Vegas, USA, January 9-12, 2016.

[31] Yang Zheng, Yuzhang Zang and Kaveh Pahlavan, UWB Localization Modeling for Electronic Gaming, IEEE International Conference on Consumer Electronics (ICCE), Las Vegas, USA, January 9-12, 2016.

[32] Lin Yao, Fang Ma and Shihong Duan, "An Object Reconstruction Algorithm for Moving Vehicle Detection Based on Three-frame Differencing, The Workshop of IEEE 2015 Smart World Congress, Beijing, China, August 10-14, 2015.

[33] Guanxiong Liu, Yishuang Geng and Kaveh Pahlavan, "Direction Estimation Error Model of Embeded Magnetometer in Indoor Navigation Environment, The Workshop of IEEE 2015 Smart World Congress, Beijing, China, August 10-14, 2015.

[34] Dan Liu, Yishuang Geng, Guanxiong Liu, Mingda Zhou and Kaveh Pahlavan, "WBANs-Spa: An Energy Efficient Relay Algorithm for Wireless Capsule Endoscopy, IEEE 82nd Vehicular Technology Conference (VTC), Boston, USA, September 6-9, 2015.

[35] Dan Liu, Mingda Zhou, Yishuang Geng and Kaveh Pahlavan, "Power Efficient Relay Networking for BANs in Non-Homogeneous Environment, The Workshop of IEEE 2015 Smart World Congress, Beijing, China, August 10-14, 2015.

[36] Yishuang Geng and Kaveh Pahlavan, "On the Accuracy of RF and Image Processing Based Hybrid Localization for Wireless Capsule Endoscopy", IEEE Wireless Communications and Networking Conference (WCNC), New Orleans, USA, March 9-12, 2015.

[37] Guanxiong Liu, Kaveh Pahlavan and Yishuang Geng, "Effects of Calibration RFID Tags on Performance of Inertial Navigation in Indoor Environment", IEEE International Conference on Computing, Networking and Communications (ICNC), Anaheim, USA, February 16-19, 2015.

[38] N. Bargshady, K. Pahlavan and N. Alsindi, "Hybrid Wifi/UWB, Cooperative Localization Using Particle Filter", IEEE International Conference on Computing, Networking and Communications (ICNC), Anaheim, USA, February 16-19, 2015.

[39] Yongtao Ma, Kaveh Pahlavan and Yishuang Geng, "Comparison of POA and TOA Based Ranging Behavior for RFID Application", IEEE 25th International Symposium on Personal, Indoor and Mobile Radio Communications (PIMRC'14), Washington, D.C, September 2-5.

[40] Jie He, Yishuang Geng, Cheng Xu, Zhishuai Han and Shihong Duan, "Height Dependent TOA Ranging Error Model for Near Ground Localization Applications", IEEE 25th International Symposium on Personal, Indoor and Mobile Radio Communications (PIMRC'14), Washington, D.C, September 2-5.

[41] Kaveh Pahlavan, "From WLAN to Wi-Fi Localization - Evolution of a Revolutionary Technology", keynote speech, International Symposium on Wireless Sensor Networks, Tokyo, Japan, June 27, 2014.

[42] Guanqun Bao, Liang Mi, Yishuang Geng, Mingda Zhou and Kaveh Pahlavan, "A Video-based Speed Estimation Technique for Localizing the Wireless Capsule

Endoscope inside Gastrointestinal Tract", the 36th Annual International Conference of the IEEE Engineering in Medicine and Biology Society (EMBC'14), Chicago, USA, August 26-30, 2014.

[43] Mingda Zhou, Guanqun Bao, and Kaveh Pahlavan, "Measurement of Motion Detection of Wireless Capsule Endoscope Inside Large Intestine", the 36th Annual International Conference of the IEEE Engineering in Medicine and Biology Society (EMBC'14), Chicago, USA, August 26-30, 2014.

[44] Liang Mi, Guanqun Bao, and Kaveh Pahlavan, "Analysis of the Impact of Intestinal Motility on the Speed Estimation of Video Capsule Endoscope", the 36th Annual International Conference of the IEEE Engineering in Medicine and Biology Society (EMBC'14), Chicago, USA, August 26-30, 2014.

[45] K. Pahlavan, V. Motevalli and A.H.Levesque, "Project Based Learning in Engineering Education for the Third Industrial Revolution", Interntional Symposium on University Globalization, Tokyo, Japan, June 28, 2014.

[46] K. Pahlavan, V. Motevalli and A.H.Levesque, "Role of Project-Based Learning and Entrepreneurship in the Evolution of Engineering Education", IACEE 14th World Conference on Continuing Engineering Education, Stanford University, June 24-27, 2014.

[47] L. Mi, G. Bao and K. Pahlavan, "Geometric Estimation of Intestinal Contraction for Motion Tracking of Video Capsule Endoscope", SPIE Medical Imaging 2014: Image-Guided Procedures, Robotic Interventions, and Modeling, San Diego, USA, February 15-20, 2014.

[48] J. Chen, Y. Ye and K. Pahlavan, "Comparison of UWB and NB RF ranging measurements in homogenous tissue for BAN applications", IEEE Wireless Telecommunications Symposium, April 17-19, 2013.

[49] G. Bao and K. Phalavan, "Motion Estimation of the Endoscopy Capsule using Region-based Kernel SVM Classifier", Electro/Information Technology (EIT), 2013 IEEE International Conference on, Rapid City, SD, May 9-11, 2013.

[50] G. Bao, L. Mi and K. Phalavan, "Emulation on Motion Tracking of Endoscopic Capsule inside Small Intestine", 2013 World Congress in Computer Science,Computer Engineering, and Applied Computing (WORLDCOMP'13), Las Vegas, USA, 2013.

[51] R. Fu, G. Bao and K. Pahlavan, "Activity Classification with Empirical RF Propagation Modeling", 8th International Conference on Body Area Networks, Boston, MA, USA, September 30-October 2, 2013

[52] G. Bao, L. Mi and K. Phalavan, "A Video Aided RF Localization Technique for the Wireless Capsule Endoscope (WCE) inside Small Intestine", the 8th International Conference on Body Area Networks, Boston, MA, USA, September 30-October 2, 2013.

[53] L. Mi, G. Bao and K. Phalavan, "Design and Validation of a Virtual Environment for Experimentation inside the Small Intestine", the 8th International Conference on Body Area Networks, Boston, MA, USA, September 30-October 2, 2013.

[54] Y. Geng, J. He, H. Deng and Kaveh Pahlavan, "Modeling the Effect of Human Body on TOA Ranging for Indoor Human Tracking with Wrist Mounted Sensor", IEEE 16th Wireless Personal Multimedia Communications Symposium (WPMC).